

The role of volatile exsolution and sub-solidus fluid/rock interactions in producing high $^{56}\text{Fe}/^{54}\text{Fe}$ ratios in siliceous igneous rocks [☆]

Adriana Heimann ^{*}, Brian L. Beard, Clark M. Johnson

Department of Geology and Geophysics, University of Wisconsin-Madison, 1215 West Dayton Street, Madison, WI 53706, USA

Received 18 February 2008; accepted in revised form 6 June 2008; available online 24 June 2008

Abstract

Highly differentiated igneous rocks can, in some cases, have $^{56}\text{Fe}/^{54}\text{Fe}$ ratios that are significantly higher than those of mafic- to intermediate-composition igneous rocks. Iron isotope compositions were obtained for bulk rock, magnetite, and Fe silicates from well-characterized suites of granitic and volcanic rocks that span a wide range in major- and trace-element contents. Sample suites studied include granitoids from Questa, N.M. (Latir volcanic field) and the Tuolumne Intrusive Series (Sierra Nevada batholith), and volcanic rocks from Coso, Katmai, Bishop Tuff, Grizzly Peak Tuff, Seguam Island, and Puyehue volcano. The rocks range from granodiorite to high-silica granite and basalt to high-silica rhyolite. The highest $\delta^{56}\text{Fe}$ values (up to +0.31‰) are generally restricted to rocks that have high Rb (>100 ppm), Th (>~15 ppm) and SiO_2 (>70 wt.%) but low Fe (<2 wt.% total Fe as Fe_2O_3) contents. Magnetite separated from these rocks has high $\delta^{56}\text{Fe}$ values, whereas Fe silicates have $\delta^{56}\text{Fe}$ values close to zero. Although in principle crystal fractionation might explain the high $\delta^{56}\text{Fe}$ values, trace-element ratios in high- $\delta^{56}\text{Fe}$ igneous rocks indicate that crystal fractionation is an unlikely explanation. The highest $\delta^{56}\text{Fe}$ values occur in volcanic and plutonic rocks that contain independent evidence for fluid exsolution, including sub-chondritic Zr/Hf ratios, suggesting that loss of a low- $\delta^{56}\text{Fe}$ ferrous chloride fluid is the most likely explanation for the high $\delta^{56}\text{Fe}$ values in the bulk rocks. Based on magnetite solubility in chloride solutions and predicted Fe isotope fractionations among Fe silicates, magnetite, and ferrous chloride fluids, the increase in $\delta^{56}\text{Fe}$ values of bulk rocks may be explained by isotopic exchange between magnetite and FeCl_2^0 , which predicts an increase in the $\delta^{56}\text{Fe}$ values of magnetite upon fluid exsolution. This model is consistent with the $\delta^{56}\text{Fe}$ values measured in this study for bulk rocks, as well as magnetite and Fe silicates. Our results suggest that fluid exsolution from siliceous hydrous magmas, which sometimes produce porphyry-style Cu, Mo, or Cu-Au mineralization, may be traced using Fe isotopes.

© 2008 Elsevier Ltd. All rights reserved.

1. INTRODUCTION

Significant variations in the stable isotope compositions of intermediate-mass elements have been demonstrated for high-temperature igneous rocks, although our understand-

ing of the origin of these variations remains limited. In the case of Fe, most igneous rocks have a homogeneous Fe isotope composition within analytical uncertainties (Beard et al., 2003a; Beard and Johnson, 2006), with the exception of mantle xenoliths (Beard and Johnson, 2004; Williams et al., 2005; Weyer et al., 2005), carbonatites (Johnson and Beard, 2006a), and some high-silica granitoids (Poitrasson and Freyrier, 2005; Schoenberg and von Blanckenburg, 2006). In the case of granitic rocks that have anomalously high $^{56}\text{Fe}/^{54}\text{Fe}$ ratios relative to more mafic igneous rocks, identifying the origin of such compositions is important to our understanding of continental crust

[☆] This is a revised version of the original manuscript after the suggestions from the Associate Editor Dr. Ripley, and the two reviewers, H. Williams and M. Sharma, resubmitted on June 3, 2008.

^{*} Corresponding author.

E-mail address: aheimann@geology.wisc.edu (A. Heimann).

processes that are commonly linked to the generation of mineralizing magmatic/hydrothermal fluids and resulting ore deposits (e.g., Simon et al., 2004).

Two hypotheses have been proposed to explain the origin of high- $^{56}\text{Fe}/^{54}\text{Fe}$ igneous rocks: (1) an origin through fractional crystallization (Schoenberg and von Blanckenburg, 2006; Schuessler et al., 2007; Huang et al., 2007), and (2) exsolution of Fe^{2+} -rich, reduced deuteric fluids from crystallizing plutons (Poitrasson and Freyrier, 2005). The first mechanism assumes significant mineral-melt Fe isotope fractionations in pure magmatic melts, which in turn has broad implications for Fe isotope fractionation during magmatic processes in the Earth's crust. The second mechanism involves fractionation of Fe isotopes in evolved, chloride-rich magma-volatile systems, which would have implications for the origin and evolution of magmatic/hydrothermal fluids and the formation of porphyry Mo or Cu mineral deposits.

Here we present a detailed Fe isotope study of siliceous igneous rocks to evaluate the origin of the high $^{56}\text{Fe}/^{54}\text{Fe}$ ratios that are found in some, but not all, high-silica (>70 wt.% SiO_2) igneous rocks. We present high-precision ($\pm 0.08\text{‰}$, 2 standard deviations, 2-SD) Fe isotope compositions of bulk rocks, magnetite, and Fe silicates from granitic and volcanic rocks from a number of well-characterized suites. Crystal fractionation as a mechanism for producing the measured Fe isotope compositions is evaluated in detail, and we conclude that this mechanism is not a likely explanation of the data. Through study of volcanic and plutonic rocks that contain independent evidence for large-scale exsolution of fluids, we conclude that loss of low- $^{56}\text{Fe}/^{54}\text{Fe}$ ferrous chloride (FeCl_2^0 ; e.g., Chou and Eugster, 1977) fluids is the best explanation for the high- $^{56}\text{Fe}/^{54}\text{Fe}$ ratios measured in some evolved igneous rocks. This study suggests that transition-metal stable isotope compositions of hydrothermal mineral deposits hosted in siliceous igneous rocks, such as porphyry-style mineralization, may be useful in constraining fluid loss processes in magmatic/hydrothermal ore deposits.

2. SAMPLE SELECTION AND DESCRIPTION

A wide variety of plutonic and volcanic rocks was selected for Fe isotope analysis to encompass a range of chemical compositions, including some that are highly differentiated (Table 1 and Fig. 1). Data from previous studies that included siliceous plutonic and volcanic rocks analyzed for Fe isotopes are also integrated into the dataset (Electronic Annex Table EA-1). The possibility that pre-eruptive exsolution of volatiles may affect Fe isotope compositions was tested through investigation of volcanic suites that had been previously studied in terms of their volatile contents and crystallization temperatures (Tables 1 and 2). The volcanic suites studied include: three volcanic rocks from the Oligocene Grizzly Peak Tuff, Colorado (Fridrich, 1987); eight Pleistocene-Recent rocks from Seguam Island, Aleutian Islands, that range from basalt to rhyolite (Jicha et al., 2005); two Recent dacite and rhyodacite samples from the Puyehue Volcano, Chilean Andes (Jicha et al., 2007); three Bishop Tuff high-silica pumice, California (Hildreth, 1979); six Pleistocene high-silica obsidians from

the Coso volcanic field, California (Bacon et al., 1981); and five dacite and high-silica rhyolite samples from the 1914 Katmai eruption, Alaska (Hildreth, 1983). Other samples studied include one high-silica Glass Mountain rhyolite, California (Metz and Mahood, 1991), and one high-silica rhyolite from the Big Pine volcanic field, California (Beard and Glazner, 1995; Beard and Johnson, 1997). Continental basalts analyzed by Beard et al. (2003b) were used as representative of the Fe isotope composition of the mafic continental crust. Plutonic rocks that recorded a variety of sub-solidus cooling and alteration histories, based primarily on O isotope data, were studied to test possible effects of sub-solidus fluid exsolution on Fe isotope compositions. The studied suites include sixteen granitic rocks from the Tertiary Latir volcanic field near Questa, New Mexico (e.g., Johnson et al., 1989, 1990) and seven granitoids from the Late Cretaceous Tuolumne Intrusive Series (TIS), Sierra Nevada, California (Bateman and Chappell, 1979; Lackey, 2005). These new data are compared with previously published data, including ten plutonic rocks from the Bergell intrusion (Central Alps, Schoenberg and von Blanckenburg, 2006), four volcanic rocks from the Lassen Volcanic field, California (Beard and Johnson, 2004), and other isolated localities (Beard et al., 2003a; Poitrasson et al., 2004; Dauphas et al., 2004; Poitrasson and Freyrier, 2005; Poitrasson, 2006; Rouxel et al., 2003, 2005; Weyer et al., 2005; Dauphas and Rouxel, 2006) from which only one sample was analyzed. All iron isotope compositions were normalized to a constant $^{56}\text{Fe}/^{54}\text{Fe}$ value for the IRMM-014 standard to avoid inter-laboratory bias. All Fe isotope compositions are reported relative to the average of igneous rocks (see Beard et al., 2003a and Electronic Annex Tables EA-1 and EA-2 for details). Chemical and Fe isotope compositions of all samples considered in this study are reported in Electronic Annex Tables EA-1 and EA-2.

The volcanic and plutonic rocks studied range from basalt to high-silica rhyolite and granodiorite to high-silica granite, and contain a wide range of Fe contents (Fig. 1). Because major-element compositions are insensitive to the extent of differentiation for granite-minimum compositions, the relative degree of evolution for silicic samples is best assessed using incompatible trace elements. Because Rb was the most commonly analyzed incompatible element in the samples considered in this study, we cast our discussion below on the role of crystal fractionation in Fe isotope fractionation in terms of Rb contents. Approximately 90% of the samples have been measured for Th contents and a positive correlation exists between Rb and Th contents (average $R^2 = 0.7$; see data in Electronic Annex Table EA-1) indicating that Rb is a reliable index for differentiation and was relatively unaffected by fractionation of alkali feldspar or micas. Samples from different petrogenetic suites were specifically chosen to cover a range in Rb contents (Fig. 1).

3. ANALYTICAL METHODS AND NOMENCLATURE

Bulk-rock powders and mineral separates were dissolved in a mixture of concentrated HF and HNO_3 in

Table 1
Bulk-rock compositions, Fe isotope compositions, and temperatures of igneous rocks analyzed in this study

| Sample | SiO ₂ (wt.%) | Fe ₂ O ₃ ^a (wt.%) | Sr (ppm) | Rb (ppm) | Zr/Hf | T ^b (°C) | δ ¹⁸ O WR (‰) | δ ⁵⁶ Fe WR ^c (‰) |
|--|----------------------------|---|-------------|-------------|-------|---------------------|-----------------------------|---|
| Intrusive Rocks | | | | | | | | |
| <i>Questa Volcanic Field, New Mexico</i> | | | | | | | | |
| <i>Sulfur Gulch Dikes, Mineralized</i> | | | | | | | | |
| Q82J-5 Porphyry (rhyolite) dike | 77.82 | 0.71 | 66.0 | 232 | | | 1.80 | 0.25 ± 0.06 |
| Q82J-6 Granodiorite | 77.60 | 0.72 | | | | | | 0.25 ± 0.02 |
| <i>Rio Hondo Pluton</i> | | | | | | | | |
| Q82-J-8 Granodiorite | 71.75 | 2.35 | 520 | 72.0 | | 625 | 6.70 | 0.09 ± 0.03 |
| Q82J-12 Granodiorite | 68.50 | 3.52 | 585 | 77.0 | | 696 | 0.70 | 0.03 ± 0.03 |
| Q82J-33 Granite | 76.31 | 1.15 | 132 | 154 | | 572 | 5.20 | 0.17 ± 0.10 |
| Q82J-34 Granite | 76.12 | 1.30 | 177 | 152 | | 587 | 5.40 | 0.13 ± 0.02 |
| Q82J-35 Granodiorite | 68.43 | 3.57 | 615 | 77.0 | | 603 | 2.90 | 0.07 ± 0.07 |
| Q83J-99 Granite | 76.91 | 0.88 | 105 | 146 | | 668 | 7.60 | 0.14 ± 0.08 |
| Q83J-101 Granodiorite | 68.40 | 3.42 | 745 | 66.0 | 47.47 | 711 | 5.80 | 0.00 ± 0.02 |
| <i>Rio Hondo Dikes</i> | | | | | | | | |
| Q82J-9 Porphyry (rhyolite) dike | 74.16 | 1.61 | 295 | 129 | | 711 | 3.00 | 0.09 ± 0.01 |
| <i>Sulfur Gulch pluton, Mineralized</i> | | | | | | | | |
| Q82J-36 Granite | 77.06 | 0.78 | 51.0 | 214 | | | 5.10 | 0.20 ± 0.02 |
| 82-QC-56 Granite | 77.20 | 0.89 | 35.5 | 183 | | | | 0.15 ± 0.07 |
| <i>Lucero Peak Pluton</i> | | | | | | | | |
| Q82J-46 Granite | 75.61 | 1.14 | 91.0 | 174 | | | 7.40 | 0.15 ± 0.06 |
| 82-QC-15 Granite | 76.83 | 1.03 | 101 | 189 | 23.42 | | 8.00 | 0.11 ± 0.02 |
| <i>Bear Canyon Pluton, Mineralized</i> | | | | | | | | |
| 82-QC-8 Granite | 77.42 | 0.68 | 43.5 | 223 | 18.99 | | 7.10 | 0.19 ± 0.04 |
| Q82J-37 Granite | 77.40 | 0.79 | 36.0 | 248 | | | | 0.30 ± 0.01 |
| <i>Red River Complex, Mineralized</i> | | | | | | | | |
| Q82J-13 Granite | 71.89 | 1.98 | 211 | 116 | | | 6.30 | 0.10 ± 0.07 |
| 82-QC-32C Peralkaline granite | 76.04 | 0.84 | 20.0 | 175 | 20.30 | | | 0.27 ± 0.05 |
| 82-QC-44 Granodiorite | 65.83 | 4.59 | 795 | 73.0 | 32.86 | | 5.60 | 0.09 ± 0.03 |
| Tuolumne Intrusive Suite, Sierra Nevada | | | | | | | | |
| <i>Kuna Crest Tonalite</i> | | | | | | | | |
| 1S108-kk | 57.64 | 7.14 | 580 | 107 | | 503-656 | 7.44 | 0.00 ± 0.01 |
| 1S106-kk | 62.67 | 5.75 | 475 | 125 | | 533-656 | 7.74 | -0.01 ± 0.05 |
| <i>Half Dome Granodiorite</i> | | | | | | | | |
| 1S105-khd | 68.72 | 3.04 | 417 | 141 | | 528-685 | 8.11 | 0.01 ± 0.06 |
| <i>Porphyritic Half Dome Granodiorite</i> | | | | | | | | |
| 1S110-khdp | 69.52 | 2.63 | 408 | 146 | | 583-657 | 8.39 | 0.00 ± 0.01 |
| <i>Cathedral Peak Granodiorite</i> | | | | | | | | |
| 1S113-kcp | 69.54 | 2.33 | 597 | 138 | | 563-650 | 8.20 | 0.04 ± 0.00 |
| 1S101-kcp | 71.46 | 1.62 | 580 | 122 | | 541-690 | 8.08 | 0.05 ± 0.01 |
| <i>Johnson Granite Porphyry</i> | | | | | | | | |
| 1S115-kj | 76.13 | 0.61 | 109 | 213 | | 515-610 | 9.13 | 0.19 ± 0.01 |
| Extrusive Rocks | | | | | | | | |
| <i>Grizzly Peak Tuff</i> | | | | | | | | |
| FG-3 (MA-1TZ) Dacite | 72.70 | 1.30 | 367 | 143 | 28.93 | 800 | 8.01 | 0.01 ± 0.09 |
| FG-5 (ZX-4) Andesite | 61.70 | 5.80 | 992 | 77.5 | 39.42 | 900 | 4.10 | 0.00 ± 0.04 |
| FG-7 (ZB-2) Andesite | 57.90 | 8.90 | 1037 | 62 | 33.90 | 900 | 7.30 | 0.02 ± 0.02 |
| Seguam Island, Aleutian Islands | | | | | | | | |
| SEG 03 44 Dacitic ash flow tuff | 64.50 | 6.15 | 228 | 42.3 | 35.68 | | | 0.01 ± 0.01 |
| SEG 03 45 Andesitic lava flow | 62.40 | 7.41 | 227 | 38.1 | 37.08 | 825 | | -0.07 ± 0.10 |
| SEG 03 03 Dacitic lava flow | 67.90 | 4.47 | 182 | 34.8 | 32.11 | 856 | | 0.04 ± 0.04 |
| SB 87 56 Rhyolitic lava flow | 71.00 | 4.91 | 175 | 52.5 | 34.51 | 776 | | -0.04 ± 0.04 |
| SEG 03 01 Rhyolite | 70.40 | 3.40 | 131 | 38.8 | 32.22 | | | 0.08 ± 0.04 |

(continued on next page)

Table 1 (continued)

| Sample | SiO ₂ (wt.%) | Fe ₂ O ₃ ^a (wt.%) | Sr (ppm) | Rb (ppm) | Zr/Hf | T ^b (°C) | δ ¹⁸ O WR (‰) | δ ⁵⁶ Fe WR ^c (‰) |
|--|----------------------------|---|-------------|-------------|-------|---------------------|-----------------------------|---|
| SEG 03 43 Rhyodacite | 68.30 | 5.35 | 163 | 38.8 | 31.20 | 791 | | 0.07 ± 0.02 |
| SEG 03 08 Basalt | 51.17 | 9.83 | 315 | 11.7 | 36.92 | 1160 | | 0.00 ± 0.05 |
| SEG 03 31 Rhyolite | 71.40 | 3.87 | 130 | 51.4 | 36.29 | 860 | | 0.07 ± 0.02 |
| Puyehue Volcano, Chilean Andes | | | | | | | | |
| PU 03 27 Dacite | 66.50 | 6.95 | 196 | 57.0 | 41.25 | >900 | | 0.05 ± 0.04 |
| PU 02 29 Rhyodacite | 69.50 | 4.98 | 168 | 70.0 | 40.60 | >900 | | 0.08 ± 0.02 |
| 1912 Katmai Eruption, Alaska | | | | | | | | |
| K-88 Initial rhyolite pumice fall, layer A | 77.40 | 1.38 | 70.5 | 57.0 | | | | −0.03 ± 0.04 |
| K-7A Rhyolite pumice, valley ignimbrite | 77.70 | 1.35 | 91.0 | 79.0 | 31.13 | | | 0.06 ± 0.02 |
| K-22 Rhyolite lava, Novarupta dome | 76.60 | 1.64 | 58.0 | 71.0 | 28.08 | | | 0.10 ± 0.01 |
| K-45 Dacite pumice, layer C | 64.60 | 5.80 | 237 | 38.0 | 33.56 | | | −0.02 ± 0.07 |
| K-54 Dacite pumice, layer G | 65.60 | 5.68 | 252 | 35.0 | 35.78 | | | −0.06 ± 0.04 |
| Coso Rhyolites-Obsidians, California (Dome #/ Group #) | | | | | | | | |
| Coso # 4/7 | 77.00 | 1.01 | | 250 | 19.39 | | | 0.23 ± 0.04 |
| Coso # 5/4 | 76.90 | 0.89 | 1.4 | 370 | 16.13 | | | 0.31 ± 0.02 |
| Coso # 14/3 | 76.60 | 1.04 | 3.7 | 315 | 17.54 | | | 0.29 ± 0.05 |
| Coso # 20/5 | 76.40 | 1.02 | 6.8 | 270 | 20.75 | | | 0.27 ± 0.05 |
| Coso # 25/6 | 76.70 | 1.10 | 10.2 | 210 | 26.47 | | | 0.21 ± 0.07 |
| Coso # 26/7 | 76.40 | 0.88 | 4.8 | 255 | 17.65 | | | 0.04 ± 0.06 |
| Bishop Tuff Pumice, California | | | | | | | | |
| B-670 Early, Pumice fall, unit F1 | 77.40 | 0.70 | 18.5 | 177 | 19.88 | | | 0.14 ± 0.07 |
| B-657 Mid, Pumice Fall, unit F6 | 75.70 | 0.81 | 16.5 | 172 | 23.08 | | | 0.18 ± 0.06 |
| B-659 Late, Pumice Fall, unit F9 | 75.50 | 0.89 | 28.3 | 164 | 24.50 | | | 0.12 ± 0.01 |
| Various Volcanic Rocks | | | | | | | | |
| RGM-1-Glass Mountain Rhyolite (USGS) | 73.40 | 1.86 | 110 | 150 | 35.71 | 695-718 | | 0.07 ± 0.07 |
| BP 9220D-Big Pine Volcanics Rhyolite | 75.81 | 0.98 | 7.6 | 196 | | | | 0.20 ± 0.02 |

^a Fe₂O₃ as total Fe; WR whole rock.

^b Temperatures for Questa granitoids calculated based on Qtz–Mgt δ¹⁸O data from Hagstrum and Johnson (1986) and the calibration of Clayton and Kieffer (1991); TIS temperatures provided by J.S. Lackey calculated from Quartz–Zircon and Zircon–Titanite δ¹⁸O thermometry (Lackey, 2005) with calibrations of Valley et al. (2003). Fe–Ti temperatures for volcanic rocks as follows: Segua Island, provided by B.R. Jicha and calculated using the algorithm of Ghiorso and Sack (1995); those from Puyehue are an estimate based on rocks of similar age and composition from the Cordon–Caulle region (Gerlach et al., 1988); Grizzly Peak for rocks from the same fiamme group as those analyzed for Fe isotopes; from Johnson and Fridrich (1990); RGM Glass Mountain rhyolite from Metz and Mahood (1991). Data for the Grizzly Peak, Katmai, and Bishop Tuffs correspond to pumice/fiamme separated from the bulk rocks (e.g., lithic fragments are not included) and the minerals are from the separated pumice/fiamme as well.

^c Iron isotope data reported (relative to igneous rocks) correspond to the average of multiple analyses of each sample, in most cases. Errors for δ⁵⁶Fe correspond to 2 standard deviation errors for samples analyzed more than one time and 2 standard errors from in-run statistics for samples analyzed only once. See Electronic Annex Table EA-1 for references and details about bulk-rock major and trace-element compositions and Table 3 and Electronic Annex Table EA-5 for the complete set of Fe isotope data.

Savillex beakers on a hotplate at ~160 °C. Dissolved samples were converted to chloride form using 8 M HCl and solutions were observed under the microscope to ensure that the entire sample had dissolved and that no fluorides were present. Iron (25 to 100 μg of Fe) from samples was purified using anion exchange resin (Bio-Rad AG 1X4 200–400 mesh resin) and HCl (e.g., Beard et al., 2003a). Iron yields from this ion-exchange chromatography were quantitative (100 ± 7%) as determined by analysis of total Fe concentration using the *Ferrozine* method (Stookey, 1970).

Iron isotope measurements were conducted using a Micromass *IsoProbe* MC-ICP-MS operated at resolving power of ~400. A micro-concentric desolvating nebulizer aspirating at ~60 μL/min was used to introduce samples into the mass spectrometer. The mass-analysis procedure followed that of Beard et al. (2003a) and Beard and

Johnson (2004), although to increase the precision of Fe isotope ratio measurements, 600 ppb Fe solutions were used. Approximately 300 ng of Fe was consumed for each analysis. Isotopic data are reported as ⁵⁶Fe/⁵⁴Fe and ⁵⁷Fe/⁵⁴Fe ratios in standard delta (δ) notation, in units of per mil (‰), and using the average of igneous rocks as the standard reference reservoir (Beard et al., 2003a):

$$\delta^{56}\text{Fe} = [({}^{56}\text{Fe}/{}^{54}\text{Fe})_{\text{sample}}/({}^{56}\text{Fe}/{}^{54}\text{Fe})_{\text{standard}} - 1] \cdot 10^3, \quad (1)$$

and

$$\delta^{57}\text{Fe} = [({}^{57}\text{Fe}/{}^{54}\text{Fe})_{\text{sample}}/({}^{57}\text{Fe}/{}^{54}\text{Fe})_{\text{standard}} - 1] \cdot 10^3. \quad (2)$$

The external precision (2-SD) for δ⁵⁶Fe values using this method is ±0.08‰. This precision is the average 2-SD calculated from: (1) multiple Fe isotope analyses of ultrapure Fe solutions [UW J-M Fe: δ⁵⁶Fe = +0.25 ± 0.06‰,

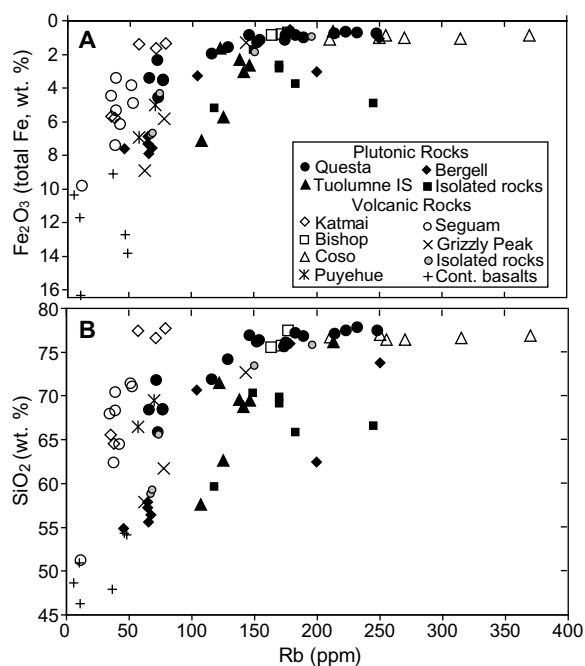


Fig. 1. (A) Plot of bulk-rock Rb (ppm) versus Fe_2O_3 (total Fe, wt.%) that shows the composition of plutonic and volcanic rocks from various petrogenetic suites and isolated localities analyzed in the present and previous studies. (B) Plot of bulk-rock Rb (ppm) versus SiO_2 (wt.%) for all the studied rocks. For clarity, in this and subsequent Figures plutonic rocks are represented by black filled symbols and volcanic rocks by open or light grey symbols. Data sources for all major- and trace-element chemical compositions used in (A) and (B) are reported in Electronic Annex Table EA-1.

Table 2

Ranges of temperatures and Cl/F ratios for Katmai, Coso, and Bishop Tuff samples

| | Cl/F MI ^a | Cl/F WR ^b | T^c (°C) |
|--------------------------------|----------------------|----------------------|------------|
| 1912 Katmai Eruption, Alaska | 3.69–4.88 | 1.75–2.75 | 805–955 |
| Coso Rhyolites-Obsidians | 0.20–0.77 | 0.20–0.66 | 743–768 |
| Bishop Tuff Pumice, California | 1.70–2.39 | 0.67–0.83 | 722–790 |

^a MI melt inclusions. Data for Cl/F in MI and bulk rocks are from Macdonald et al. (1992), Mahood and Hildreth (1983), Manley and Bacon (2000), Wallace et al. (1999), and Westrich et al. (1991) and were not analyzed for the same samples that were analyzed for Fe isotopes. However, the ranges shown correspond to rocks of similar composition as the ones analyzed for Fe isotopes.

^b WR whole rock.

^c Temperature ranges for Coso, Bishop Tuff, and Katmai are from Manley and Bacon (2000), Mahood and Hildreth (1983), and Hildreth (1983), respectively, from rocks of similar compositions and derived from the same units as those analyzed for Fe isotopes.

$\delta^{57}\text{Fe} = +0.38 \pm 0.11\text{‰}$ ($n = 55$); HPS Fe: $\delta^{56}\text{Fe} = +0.49 \pm 0.08\text{‰}$, $\delta^{57}\text{Fe} = +0.74 \pm 0.10\text{‰}$ ($n = 55$); IRMM-0–14 Fe: $\delta^{56}\text{Fe} = -0.08 \pm 0.06\text{‰}$, $\delta^{57}\text{Fe} = -0.12 \pm 0.11\text{‰}$ ($n = 65$), (2) 27 analyses of 13 HPS Fe solutions that were processed through the ion-exchange procedure, and yielded $\delta^{56}\text{Fe} = +0.49 \pm 0.07\text{‰}$, $\delta^{57}\text{Fe} = +0.74 \pm 0.10\text{‰}$, (3) repli-

cate analyses of eight synthetic rock solutions, which were processed through the entire analytical procedure and had an average external (2-SD) precision of $\pm 0.06\text{‰}$ for $\delta^{56}\text{Fe}$ and 0.12‰ in $\delta^{57}\text{Fe}$, and (4) the average 2-SD for 103 replicates of the 112 analyzed samples which was $\pm 0.04\text{‰}$ for $\delta^{56}\text{Fe}$ and $\pm 0.09\text{‰}$ for $\delta^{57}\text{Fe}$ (additional details in Electronic Annex Tables EA-3 and EA-4). These tests show that the external precision of the isotope ratio measurements of natural and synthetic samples with complicated matrices reproduce to the same level as ultrapure solutions not passed through the ion-exchange procedure and thus are free of any detectable matrix effects. Possible matrix effects were evaluated using artificial solutions of known Fe isotope composition that match the range in major-element compositions of our rock samples, and these tests demonstrate that accurate Fe isotope compositions may be recovered from complex matrices within the uncertainties of measurements of ultrapure standards that were not passed through chemistry (EA-3). We conclude that our Fe isotope analyses of samples are accurate and do not suffer from spectral or non-spectral interferences that can hinder isotope ratio measurements that preserve naturally occurring, mass-dependent variations (e.g., Albarède and Beard, 2004).

Fifteen samples have been analyzed by more than one laboratory (or in different studies) and there is excellent inter-laboratory agreement in the Fe isotope compositions of silicic-, mafic-, and intermediate-composition igneous rocks (see Electronic Annex Table EA-2). We completed six replicate analyses of the samples studied by Beard et al. (2003a) and several analyses of an igneous rock standard (see Tables 1 and EA-2); except for one sample, all analyses agree to within $\pm 0.07\text{‰}$. Based on these replicate analyses we conclude that there are no inter-laboratory biases in measured Fe isotope compositions. Inter-laboratory comparisons may be made through the IRMM-014 Fe standard, which has a $\delta^{56}\text{Fe}$ value of $-0.09 \pm 0.05\text{‰}$ on the igneous rock scale (Beard et al., 2003a). Note that the igneous rock scale of Beard et al. (2003a) is identical to the “mean mafic Earth” as defined by Poitrasson et al. (2004). We note that the difference in $\delta^{56}\text{Fe}$ values for the average of igneous rocks and the IRMM-014 standard has remained unchanged since it was defined by Beard et al. (2003a), and Beard and Johnson (2006) give conversion equations for $^{56}\text{Fe}/^{54}\text{Fe}$ and $^{57}\text{Fe}/^{54}\text{Fe}$ isotope ratios reported relative to the average of igneous rocks and IRMM-014 scales. Finally, we follow standard approaches in defining inter-mineral Fe isotope fractionation factors between two minerals A and B ($\alpha^{56}\text{Fe}_{A-B}$) using the following approximation:

$$\Delta^{56}\text{Fe}_{A-B} = \delta^{56}\text{Fe}_A - \delta^{56}\text{Fe}_B \approx 10^3 \ln \alpha^{56}\text{Fe}_{A-B}. \quad (3)$$

4. RESULTS

Volcanic and plutonic rocks that have SiO_2 and Fe_2O_3 (total Fe) contents of less than 70 wt.% and more than 2 wt.%, respectively, generally have whole-rock $\delta^{56}\text{Fe}$ values that lie within the range previously defined for mafic to intermediate-composition igneous rocks (Fig. 2; $\delta^{56}\text{Fe} = 0.00 \pm 0.08\text{‰}$, 2-SD; e.g., Beard and Johnson,

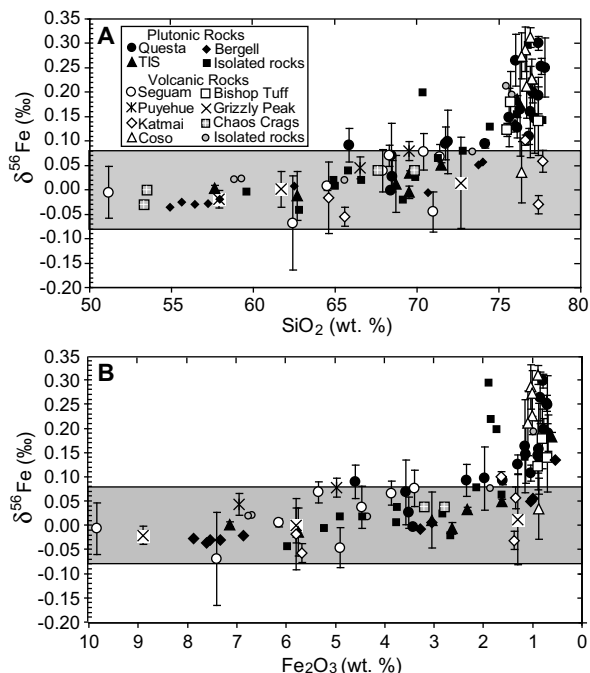


Fig. 2. (A) $\delta^{56}\text{Fe}$ (relative to igneous rocks, ‰) of bulk plutonic and volcanic rocks as a function of SiO_2 content (wt.%). The shaded area corresponds to the average Fe isotope composition and 2 standard deviation errors ($0.00 \pm 0.08\text{‰}$; 2-SD, $n = 108$) representative of the bulk crust calculated from mafic- to intermediate-composition igneous rocks from Beard et al. (2003a), Rouxel et al. (2003, 2005), Poitrasson et al. (2004), Dauphas et al. (2004), Poitrasson and Freyrier (2005), Weyer et al. (2005), Poitrasson (2006), Schoenberg and von Blanckenburg (2006), Weyer and Ionov (2007), and this study. Error bars (shown for the current study only) correspond to the 2 standard deviation errors calculated from several analyses of the same sample or the 2 standard error (from in-run statistics) if the sample was only analyzed once. (B) $\delta^{56}\text{Fe}$ versus Fe_2O_3 (wt.%, total Fe) for the same rocks. Data from this study are distinguished by larger symbols. Iron isotope data that are not from this study include analyses from Schoenberg and von Blanckenburg (2006), Beard and Johnson (2004), Beard et al. (2003a), Poitrasson and Freyrier (2005), Dauphas and Rouxel (2006), Poitrasson (2006), and Dauphas et al. (2004). Electronic Annex Tables EA-1 and EA-2 list the sample localities, compositions, and references for all the major- and trace-element data and Fe isotope compositions for samples plotted here.

2004; Poitrasson and Freyrier, 2005; this study; Table 3 and Electronic Annex Table EA-5). The largest range in $\delta^{56}\text{Fe}$ values for whole-rock samples is found in rocks that have ≥ 70 wt.% SiO_2 and ≤ 2 wt.% total Fe as Fe_2O_3 (Fig. 2). The $\delta^{56}\text{Fe}$ values for these evolved rocks range from -0.03‰ to $+0.31\text{‰}$ (Fig. 2), and the range for bulk volcanic and plutonic rocks is similar.

The $\delta^{56}\text{Fe}$ values for volcanic and plutonic rocks are positively correlated with Rb concentration (Fig. 3A), suggesting an important control on Fe isotope compositions and the extent of differentiation. That the Rb– $\delta^{56}\text{Fe}$ correlation is generally better than the SiO_2 – $\delta^{56}\text{Fe}$ or Fe_2O_3 – $\delta^{56}\text{Fe}$ correlations (Fig. 2) reflects the greater sensitivity of Rb to the extent of differentiation relative to SiO_2 and

Table 3

Fe isotope compositions of bulk rocks and minerals from igneous rocks^a

| Sample | $\delta^{56}\text{Fe}$ | $\delta^{57}\text{Fe}$ |
|--|------------------------|------------------------|
| Intrusive Rocks | | |
| <i>Questa Volcanic Field</i> | | |
| Sulfur Gulch Dikes, Mineralized | | |
| <i>Q82J-5 Porphyry dike, Mo mine</i> | | |
| WR | 0.25 ± 0.06 | 0.34 ± 0.17 |
| Chl/Bt | -0.07 ± 0.02 | -0.10 ± 0.03 |
| Mgt | 0.49 ± 0.06 | 0.70 ± 0.11 |
| <i>Q82J-6 Porphyry dike</i> | | |
| WR | 0.25 ± 0.02 | 0.36 ± 0.02 |
| Rio Hondo Pluton | | |
| <i>Q82J-8 Granite</i> | | |
| WR | 0.09 ± 0.03 | 0.10 ± 0.04 |
| Mgt | 0.11 ± 0.01 | 0.14 ± 0.05 |
| Bt | -0.01 ± 0.04 | -0.06 ± 0.03 |
| <i>Q82J-12 Granodiorite</i> | | |
| WR | 0.03 ± 0.03 | 0.09 ± 0.08 |
| Mgt | 0.10 ± 0.01 | 0.17 ± 0.03 |
| Bt | -0.11 ± 0.02 | -0.18 ± 0.01 |
| Chl | -0.12 ± 0.06 | -0.18 ± 0.06 |
| <i>Q82J-33 Granite</i> | | |
| WR | 0.17 ± 0.10 | 0.26 ± 0.18 |
| Mgt | 0.40 ± 0.02 | 0.60 ± 0.10 |
| Bt | -0.03 ± 0.09 | -0.08 ± 0.14 |
| Chl | -0.14 ± 0.02 | -0.17 ± 0.02 |
| <i>Q82J-34 Granite</i> | | |
| WR | 0.13 ± 0.02 | 0.23 ± 0.02 |
| Mgt | 0.28 ± 0.07 | 0.41 ± 0.07 |
| <i>Q82J-35 Granodiorite</i> | | |
| WR | 0.07 ± 0.07 | 0.09 ± 0.11 |
| Mgt | 0.23 ± 0.02 | 0.33 ± 0.02 |
| Bt | 0.02 ± 0.11 | 0.05 ± 0.30 |
| Chl | -0.13 ± 0.03 | -0.14 ± 0.09 |
| Hbl | -0.05 ± 0.04 | -0.05 ± 0.07 |
| <i>Q83J-99 Granite</i> | | |
| WR | 0.14 ± 0.08 | 0.17 ± 0.15 |
| Mgt | 0.21 ± 0.04 | 0.32 ± 0.12 |
| <i>Q83J-101 Granodiorite</i> | | |
| WR | 0.00 ± 0.02 | 0.00 ± 0.06 |
| Mgt | 0.14 ± 0.06 | 0.21 ± 0.17 |
| Bt | -0.02 ± 0.03 | -0.03 ± 0.06 |
| Rio Hondo Dikes | | |
| <i>Q82J-9 Porphyry (rhyolite) dike</i> | | |
| WR | 0.09 ± 0.01 | 0.15 ± 0.03 |
| Mgt | 0.24 ± 0.02 | 0.36 ± 0.10 |
| Sulfur Gulch Pluton, Mineralized | | |
| <i>Q82J-36 Granite (Mo mine)</i> | | |
| WR | 0.20 ± 0.02 | 0.30 ± 0.07 |
| Bt | 0.09 ± 0.05 | 0.13 ± 0.09 |
| <i>82-QC-56 Granite</i> | | |
| WR | 0.15 ± 0.07 | 0.23 ± 0.12 |
| Lucero Peak Pluton | | |
| <i>Q82J-46 Granite</i> | | |
| WR | 0.15 ± 0.06 | 0.20 ± 0.12 |
| Bt | 0.00 ± 0.06 | 0.07 ± 0.04 |
| Mgt | 0.19 ± 0.03 | 0.28 ± 0.07 |

Table 3 (continued)

| Sample | $\delta^{56}\text{Fe}$ | $\delta^{57}\text{Fe}$ |
|--|------------------------|------------------------|
| <i>82-QC-15 Granite</i> | | |
| WR | 0.11 ± 0.02 | 0.14 ± 0.01 |
| Bt | 0.04 ± 0.03 | 0.06 ± 0.02 |
| Bear Canyon Pluton, Mineralized | | |
| <i>82-QC-8 Granite</i> | | |
| WR | 0.19 ± 0.04 | 0.30 ± 0.04 |
| Bt | 0.03 ± 0.09 | 0.04 ± 0.15 |
| <i>Q82J-37 Granite</i> | | |
| WR | 0.30 ± 0.01 | 0.43 ± 0.10 |
| Red River Complex, Mineralized | | |
| <i>Q82J-13 Granite</i> | | |
| WR | 0.10 ± 0.07 | 0.14 ± 0.08 |
| Bt | 0.00 ± 0.08 | 0.07 ± 0.07 |
| Mgt | 0.10 ± 0.02 | 0.16 ± 0.03 |
| Hbl | -0.10 ± 0.02 | -0.15 ± 0.01 |
| <i>82-QC-32C Peralkaline (alkali fsp.) granite</i> | | |
| WR | 0.27 ± 0.05 | 0.38 ± 0.09 |
| Bt | 0.04 ± 0.06 | 0.07 ± 0.14 |
| <i>82-QC-44 Granodiorite</i> | | |
| WR | 0.09 ± 0.03 | 0.10 ± 0.02 |
| Bt | -0.14 ± 0.04 | -0.18 ± 0.03 |
| Tuolumne Intrusive Suite (WR) | | |
| Kuna Crest Tonalite | | |
| 1S108-kk | 0.00 ± 0.01 | 0.01 ± 0.02 |
| 1S106-kk | -0.01 ± 0.05 | 0.02 ± 0.15 |
| Half Dome Granodiorite | | |
| 1S105-khd | 0.01 ± 0.06 | 0.03 ± 0.00 |
| Porphyritic Half Dome Granodiorite | | |
| 1S110-khdp | 0.00 ± 0.01 | -0.01 ± 0.04 |
| Cathedral Peak Granodiorite | | |
| 1S113-kcp | 0.04 ± 0.00 | 0.06 ± 0.01 |
| 1S101-kcp | 0.05 ± 0.01 | 0.08 ± 0.18 |
| Johnson Granite Porphyry | | |
| 1S115-kj | 0.19 ± 0.01 | 0.26 ± 0.08 |
| Volcanic Rocks | | |
| Grizzly Peak Tuff | | |
| <i>FG-3 Rhyolite</i> | | |
| WR | 0.01 ± 0.09 | 0.03 ± 0.14 |
| Bt | -0.09 ± 0.09 | -0.12 ± 0.10 |
| <i>FG-5 (ZX-4) Andesite</i> | | |
| WR | 0.00 ± 0.04 | 0.00 ± 0.14 |
| Bt | -0.04 ± 0.00 | -0.04 ± 0.12 |
| <i>FG-7 (ZB-2) Andesite</i> | | |
| WR | -0.02 ± 0.02 | 0.02 ± 0.09 |
| Hbl | 0.00 ± 0.04 | 0.03 ± 0.04 |
| Seguam Island, Aleutian Islands | | |
| <i>SEG 03 44 Dacitic Ash flow tuff</i> | | |
| WR | 0.01 ± 0.01 | 0.04 ± 0.05 |
| Mgt | 0.10 ± 0.11 | 0.13 ± 0.10 |
| Gm | 0.03 ± 0.04 | 0.04 ± 0.12 |
| <i>SEG 03 45 Andesitic lava flow</i> | | |
| WR | -0.07 ± 0.10 | -0.10 ± 0.11 |
| Mgt | -0.02 ± 0.06 | -0.04 ± 0.05 |
| Gm | 0.11 ± 0.02 | 0.14 ± 0.02 |

Table 3 (continued)

| Sample | $\delta^{56}\text{Fe}$ | $\delta^{57}\text{Fe}$ |
|--|------------------------|------------------------|
| <i>SEG 03 03 Dacitic lava flow</i> | | |
| WR | 0.04 ± 0.04 | 0.07 ± 0.03 |
| Mgt | 0.06 ± 0.06 | 0.07 ± 0.10 |
| Opx | -0.05 ± 0.05 | -0.10 ± 0.04 |
| Gm | -0.02 ± 0.03 | -0.01 ± 0.02 |
| <i>SB 87 56 Rhyolitic lava flow</i> | | |
| WR | -0.04 ± 0.04 | -0.04 ± 0.06 |
| Mgt | 0.08 ± 0.09 | 0.13 ± 0.12 |
| Opx | -0.13 ± 0.02 | -0.21 ± 0.02 |
| Gm | 0.00 ± 0.03 | 0.00 ± 0.04 |
| <i>SEG 03 01 Rhyolite</i> | | |
| WR | 0.08 ± 0.04 | 0.12 ± 0.02 |
| Gm | 0.06 ± 0.03 | 0.12 ± 0.02 |
| <i>SEG 03 43 Rhyodacite</i> | | |
| WR | 0.07 ± 0.02 | 0.11 ± 0.03 |
| Opx | -0.12 ± 0.02 | -0.16 ± 0.02 |
| Mgt | 0.15 ± 0.02 | 0.24 ± 0.06 |
| Gm | 0.02 ± 0.02 | 0.02 ± 0.02 |
| <i>SEG 03 08 Basalt</i> | | |
| WR | 0.00 ± 0.05 | 0.06 ± 0.05 |
| Mgt | 0.01 ± 0.02 | 0.02 ± 0.02 |
| Gm | -0.07 ± 0.09 | -0.10 ± 0.12 |
| <i>SEG 03 31 Rhyolite</i> | | |
| WR | 0.07 ± 0.02 | 0.09 ± 0.02 |
| Mgt | 0.06 ± 0.04 | 0.12 ± 0.04 |
| Cpx | -0.13 ± 0.03 | -0.21 ± 0.03 |
| Gm | 0.09 ± 0.06 | 0.12 ± 0.04 |
| Puyehue Volcano, Chilean Andes | | |
| <i>PU 03 27 Dacite</i> | | |
| WR | 0.05 ± 0.04 | 0.06 ± 0.03 |
| Mgt | -0.05 ± 0.08 | -0.04 ± 0.19 |
| Gm | 0.03 ± 0.04 | 0.06 ± 0.04 |
| <i>PU 02 29 Rhyodacite</i> | | |
| WR | 0.08 ± 0.02 | 0.16 ± 0.12 |
| Mgt | -0.06 ± 0.02 | -0.08 ± 0.04 |
| Gm | 0.10 ± 0.04 | 0.15 ± 0.04 |
| Opx | -0.14 ± 0.09 | -0.20 ± 0.08 |
| 1912 Katmai Eruption, Alaska (WR) | | |
| K-7A Rhyolite | 0.06 ± 0.02 | 0.05 ± 0.08 |
| K-22 Rhyolite | 0.10 ± 0.01 | 0.15 ± 0.01 |
| K-45 Dacite | -0.02 ± 0.07 | -0.05 ± 0.11 |
| K-54 Dacite | -0.06 ± 0.04 | -0.09 ± 0.03 |
| K-88 Rhyolite | -0.03 ± 0.04 | -0.04 ± 0.04 |
| Coso Obsidians, California (WR) | | |
| Coso # 4/7 | 0.23 ± 0.04 | 0.33 ± 0.05 |
| Coso # 5/4 | 0.31 ± 0.02 | 0.44 ± 0.01 |
| Coso # 14/3 | 0.29 ± 0.05 | 0.45 ± 0.10 |
| Coso # 20/5 | 0.27 ± 0.05 | 0.43 ± 0.12 |
| Coso # 25/6 | 0.21 ± 0.07 | 0.31 ± 0.10 |
| Coso # 26/7 | 0.04 ± 0.06 | 0.06 ± 0.11 |
| Bishop Tuff, California (WR) | | |
| <i>B-670 Early, unit F1 Rhyolite</i> | | |
| WR | 0.14 ± 0.07 | 0.20 ± 0.13 |
| <i>B-657 Middle, Fall unit F6 Rhyolite</i> | | |
| WR | 0.18 ± 0.06 | 0.27 ± 0.10 |

(continued on next page)

Table 3 (continued)

| Sample | $\delta^{56}\text{Fe}$ | $\delta^{57}\text{Fe}$ |
|--|------------------------|------------------------|
| <i>B-659 Late, Fall unit F9 Rhyolite</i> | | |
| WR | 0.12 ± 0.01 | 0.19 ± 0.07 |
| Isolated Volcanic Rocks | | |
| RGM-1- USGS Glass Mountain Rhyolite | | |
| WR | 0.07 ± 0.07 | 0.10 ± 0.09 |
| BP 9220 D- Big Pine Volcanics Rhyolite | | |
| WR | 0.20 ± 0.02 | 0.29 ± 0.15 |

^a Data reported correspond to the average of multiple analyses of each sample, in most cases. The complete set of data appears in [Electronic Annex Table EA-5](#). Errors correspond to 2 standard errors from in-run statistics for samples analyzed only once, and 2 standard deviation errors for samples analyzed more than one time. Bt, biotite; Chl, chlorite; Cpx, clinopyroxene; fsp, feldspar; Gm, groundmass; Hbl, hornblende; Mgt, magnetite; Opx, orthopyroxene; WR, whole rock.

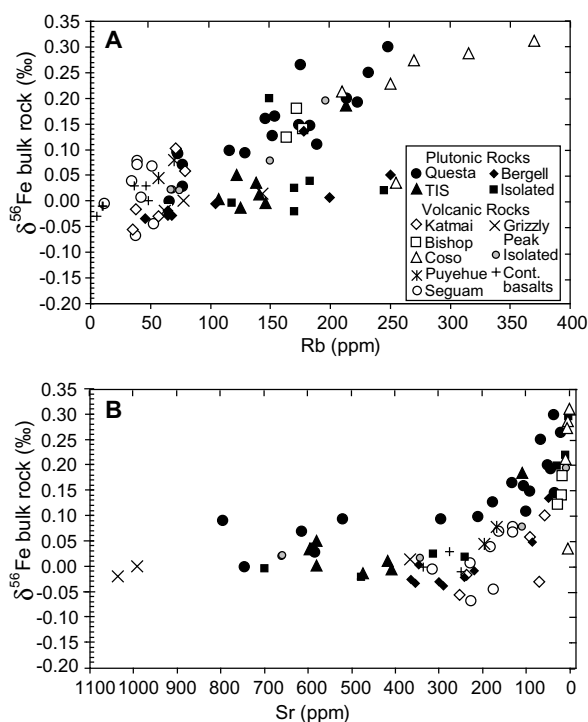


Fig. 3. Plots of (A) Rb (ppm) versus bulk-rock $\delta^{56}\text{Fe}$ (‰), and (B) Sr (ppm) versus bulk-rock $\delta^{56}\text{Fe}$ (‰) for the same rocks as in Fig. 1. References for data reported in [Electronic Annex Table EA-1](#).

Fe_2O_3 contents for high-silica rocks. Strontium– $\delta^{56}\text{Fe}$ relations (Fig. 3B) are consistent with these observations, where the most evolved rocks (low Sr, high Rb, Th) tend to have the highest $\delta^{56}\text{Fe}$ values. Among the samples analyzed in this study, the mineralized Questa plutons tend to have the highest $\delta^{56}\text{Fe}$ values for a given extent of differentiation (high Rb and Th, low Sr). It is noteworthy that the highly evolved Coso volcanic rocks have high $\delta^{56}\text{Fe}$ values that overlap those of the high-silica Questa plutons.

Silicate minerals analyzed for Fe isotopes include olivine, biotite, amphibole, and pyroxene in volcanic rocks, and biotite and hornblende in granitic rocks. These Fe sili-

cates have $\delta^{56}\text{Fe}$ values that lie within the field defined for mafic- and intermediate-composition igneous rocks, indicating little fractionation between melt and the silicate minerals, despite large decreases in total Fe contents with increasing SiO_2 contents in the bulk rocks (Fig. 4). The constant $\delta^{56}\text{Fe}$ values for silicate minerals extends to highly evolved samples, including high-silica granites. In contrast, the $\delta^{56}\text{Fe}$ values for magnetite vary significantly; and for rocks with greater than ~ 67 wt.% SiO_2 , magnetite tends to have a higher $\delta^{56}\text{Fe}$ value as compared to coexisting silicate minerals. Sufficient magnetite could be separated from dacite and low-silica rhyolites (~ 67 to ~ 72 wt.% SiO_2) to allow comparison with magnetite from granodiorites and low-silica granites; although the average $\delta^{56}\text{Fe}$ value of magnetite from plutonic rocks is slightly higher ($\delta^{56}\text{Fe} = +0.14 \pm 0.12\text{‰}$, $n = 4$) than magnetite from volcanic rocks ($\delta^{56}\text{Fe} = +0.06 \pm 0.13\text{‰}$, $n = 7$) except for sample SEG03-43, the $\delta^{56}\text{Fe}$ values overlap from $+0.02\text{‰}$ to $+0.19\text{‰}$ or within 0.17‰ (Fig. 4). Magnetite from evolved plutonic rocks (>72 wt.% SiO_2) has the highest $\delta^{56}\text{Fe}$ values ($\delta^{56}\text{Fe} = +0.26 \pm 0.11\text{‰}$, $n = 6$). Mineral separates, particularly magnetite, were not obtained from the highly evolved volcanic rocks because of their low crystal contents.

The $\delta^{56}\text{Fe}$ value of magnetite, particularly in the evolved granitic rocks, controls the magnetite–Fe silicate ($\Delta^{56}\text{Fe}_{\text{Mgt-Fe sil}}$) fractionation factor (Fig. 5A). Considering the Questa plutonic rocks for which the bulk of the magnetite–Fe silicate mineral pairs have been analyzed, the correlation between $\Delta^{56}\text{Fe}_{\text{Mgt-Fe sil}}$ and the $\delta^{56}\text{Fe}$ value of the whole rock (Fig. 5B) cannot be interpreted as a result of closed-system temperature-dependent Fe isotope exchange. In a closed system, $\Delta^{56}\text{Fe}_{\text{Mgt-Fe sil}}$ fractionations would not correlate with bulk-rock $\delta^{56}\text{Fe}$ values (Fig. 5B). Instead, the $\Delta^{56}\text{Fe}_{\text{Mgt-Fe sil}}$ fractionations and the $\delta^{56}\text{Fe}$ value of the whole rock would define a line of constant bulk-rock $\delta^{56}\text{Fe}$ values that represents closed-system cooling. We suggest that these trends in Fe isotope compositions are a result of open-system processes. Below we investigate if fractional crystallization and fluid exsolution are possible open-system methods that could produce these isotopic fractionations.

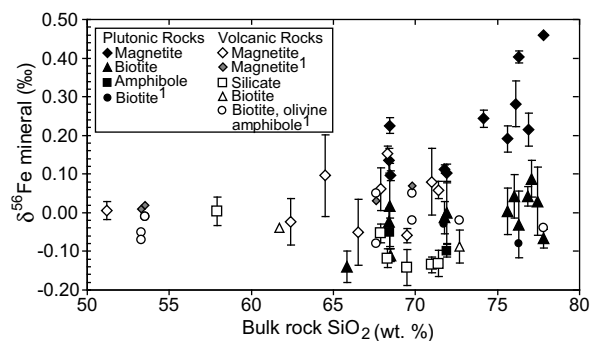


Fig. 4. Bulk-rock SiO_2 (wt.%) versus $\delta^{56}\text{Fe}$ (‰) for magnetite, biotite, and other Fe silicates (hornblende, pyroxene, olivine) from Questa granitoids and volcanic rocks from Grizzly Peak Tuff, Seguam, and Puyehue analyzed in this study and shown in Fig. 2. Silicate refers to clinopyroxene, orthopyroxene, and olivine. ¹Data from Chaos Crags, Lassen Volcanic National Park, from [Beard and Johnson \(2004\)](#) and from Grizzly Peak Tuff and Questa volcanic field from [Beard et al. \(2003a\)](#).

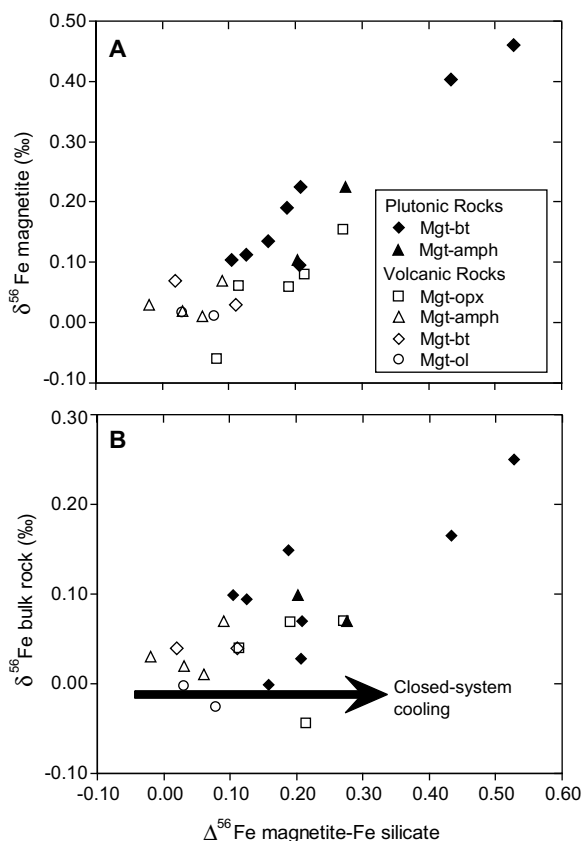


Fig. 5. (A) Calculated fractionation factors ($\Delta^{56}\text{Fe}$) for magnetite (mgt)–biotite (bt) and magnetite–amphibole (amph) in plutonic rocks and magnetite–silicates (orthopyroxene (opx), amph, bt, and olivine (ol)) in volcanic rocks versus $\delta^{56}\text{Fe}$ (‰) of magnetite. (B) $\Delta^{56}\text{Fe}$ fractionation factors for magnetite–biotite and magnetite–amphibole in plutonic rocks, and magnetite–Fe silicates in volcanic rocks versus bulk-rock $\delta^{56}\text{Fe}$ (‰). The data include eight points from Beard and Johnson (2004).

5. DISCUSSION

The origin of high $\delta^{56}\text{Fe}$ values in siliceous igneous rocks is controversial and the debate has involved two models: (1) fractional crystallization (e.g., Schoenberg and von Blanckenburg, 2006; Schuessler et al., 2007), and (2) exsolution of Fe^{2+} -bearing fluids during crystallization of plutons (Poitrasson and Freydier, 2005). We explore both of these models below, beginning with a discussion of mineral–mineral and mineral–fluid Fe isotope fractionation factors at high temperature. Crystal fractionation is first considered as an explanation for the high $\delta^{56}\text{Fe}$ values in silicic igneous rocks, followed by a discussion of fluid exsolution at magmatic and sub-solidus temperatures.

5.1. Mineral–mineral and mineral–fluid Fe isotope fractionation factors

Iron-bearing phases in the high-silica granitoids are biotite, minor hornblende, and magnetite. Biotite, the most common Fe-rich phase, contains between 12 and 25 wt.% FeO (as total Fe). Iron in magmatic/hydrothermal fluids

derived from igneous rocks is thought to be present as the FeCl_2^0 species (e.g., Chou and Eugster, 1977). We recognize that Fe speciation will exist as FeCl_2^0 in magmatic systems, and in the absence of experimental data, we assume the Fe isotope fractionation factors for FeCl_2^0 are similar to FeCl_4^{2-} .

The predicted or experimentally measured Fe isotope fractionation factors for magnetite, Fe silicate, and Fe^{2+} chloride solutions (Polyakov and Mineev, 2000; Schauble et al., 2001; Polyakov et al., 2007; Shahar et al., 2008) highlight the important control that magnetite may play in determining the Fe isotope composition of igneous rocks (Fig. 6). At the magmatic temperatures of the evolved volcanic rocks studied (~ 900 – 700 °C; Tables 1 and 2), $\Delta^{56}\text{Fe}_{\text{Mgt-Fe sil}}$ fractionations are predicted to be $\sim +0.17$ ‰ to $+0.25$ ‰ (Fig. 6). Results from recent experimental studies are in agreement with theoretical predictions and indicate magnetite–fayalite Fe isotope fractionation factors for $^{56}\text{Fe}/^{54}\text{Fe}$ between $+0.1$ ‰ and $+0.2$ ‰ at 900 and 700 °C, respectively (Shahar et al., 2008). The average modes of the Fe-bearing phenocrysts in the intermediate-composition volcanic rocks that were studied is approximately 0.1:0.6:0.3 for magnetite:clinopyroxene:orthopyroxene. Ranges in Fe contents for clinopyroxene and orthopyroxene are 12–14 wt.% FeO and 5–27 wt.% FeO, respectively, based on average contents in intermediate-composition lavas (Deer et al., 1992). Adjusting for typical ranges in Fe contents for natural mafic silicate minerals), the net mineral–melt Fe isotope fractionation factors should lie between $+0.03$ ‰ and $+0.07$ ‰ from 900 to 700 °C (Fig. 6; see Figure caption for details about the calculation).

At the oxygen isotope closure temperatures that characterize the Questa and TIS granitoids (~ 710 to ~ 500 °C; Table 1), the magnetite– Fe^{2+} chloride solution fractionations are predicted to be quite large, between $+0.3$ ‰ and $+0.5$ ‰ (Fig. 6). At the relatively fast cooling rates of the Questa and TIS rocks, we assume that Fe and O isotope exchange closed at similar temperatures, at least within 100 °C (e.g., Valaas-Hyslop et al., 2008).

5.2. Fractional crystallization

Rayleigh fractionation can potentially explain the high $\delta^{56}\text{Fe}$ values measured in some silicic volcanic rocks (Fig. 7), but only at the limits of likely $\Delta^{56}\text{Fe}_{\text{min-melt}}$ fractionation factors and distribution coefficients for Rb. In the absence of significant biotite or alkali feldspar on the liquidus during fractionation of mafic- to intermediate-composition magmas, a bulk mineral–melt distribution coefficient for Rb (D_{Rb}) near zero seems likely. Moreover, at the high temperatures associated with crystallization of mafic- to intermediate-composition magmas, the $\Delta^{56}\text{Fe}_{\text{min-melt}}$ fractionation factor is likely to be near zero, perhaps $\sim +0.03$ ‰ (Fig. 6). Under such constraints, crystal fractionation cannot produce the observed Rb– $\delta^{56}\text{Fe}$ variations (Fig. 7). If, however, the $\Delta^{56}\text{Fe}_{\text{min-melt}}$ fractionation factor was larger (~ 0.07 ‰, Fig. 6), which is possible given the uncertainties in the predicted Fe isotope fractionation factors, or if more magnetite crystallized in the rocks, the Rb– $\delta^{56}\text{Fe}$ relations seen in Fig. 7 may be produced, if the

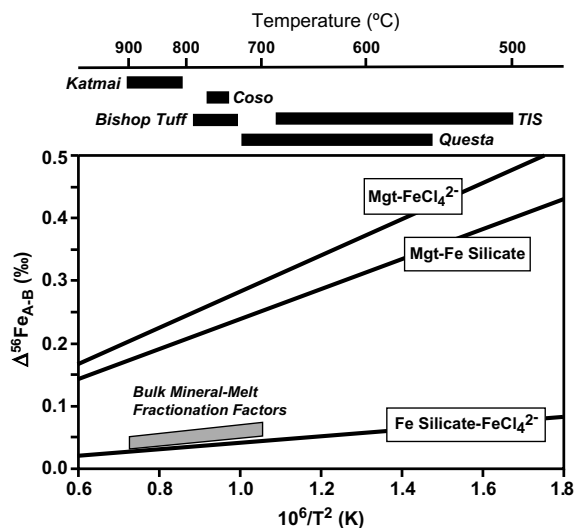


Fig. 6. Theoretical Fe isotope fractionation factors ($\Delta^{56}\text{Fe}$) as a function of temperature ($10^6/T^2$, K) for the range of temperatures (shown on top in $^\circ\text{C}$) for the studied rocks. The grey shaded area represents the mode-adjusted mineral-melt $\Delta^{56}\text{Fe}$ fractionation factors calculated based on theoretical magnetite–Fe silicate Fe isotope fractionation factors, two modal proportions of magnetite and Fe silicates of intermediate-composition igneous rocks analyzed in this study, and Fe contents in the minerals. For mode fractions of 0.1:0.6:0.3 for magnetite:clinopyroxene:orthopyroxene (mgt:cpx:opx), the $\Delta^{56}\text{Fe}$ fractionation factors are $+0.03\text{‰}$ and $+0.07\text{‰}$ at 900 and 700 $^\circ\text{C}$, respectively, whereas for modes of 0.2:0.8 for mgt:cpx the $\Delta^{56}\text{Fe}$ fractionation factors are $+0.05\text{‰}$ and $+0.07\text{‰}$ at 900 and 700 $^\circ\text{C}$, respectively. Fractionation factors were calculated by adjusting for typical ranges in Fe contents for natural mafic silicate minerals by multiplying each mineral mode by the percentage of Fe in the mineral, adding them together, and multiplying by the magnetite–Fe silicate fractionation factor at each temperature. Fractionation factors are also shown for magnetite– FeCl_4^{2-} fluid, magnetite–Fe silicate, and Fe silicate– FeCl_4^{2-} fluid. The $\Delta^{56}\text{Fe}$ fractionation factors were calculated from the coefficients of the polynomial expansions or the reduced isotopic partition function ratios (beta factors, β) of Polyakov and Mineev (2000), Schauble et al. (2001), and Polyakov et al. (2007). For Fe silicates, the average of the β factors for olivine, enstatite, and diopside of Polyakov and Mineev (2000) were used. For the fluid, beta factors for FeCl_4^{2-} were used. Temperature ranges for Coso, Bishop Tuff, and Katmai are from Manley and Bacon (2000), Mahood and Hildreth (1983), and Hildreth (1983), respectively, whereas those for Questa granitoids were calculated by magnetite–quartz oxygen isotope thermometry using $\delta^{18}\text{O}$ values from Hagstrum and Johnson (1986) and the equation of Clayton and Kieffer (1991). Temperatures for TIS were provided by J.S. Lackey and calculated based on quartz–zircon and zircon–titanite oxygen isotope thermometry with calibrations of Valley et al. (2003).

bulk D_{Rb} value is high (~ 0.5). Such a high bulk partition coefficient for Rb is possible if significant quantities of alkali feldspar or mica crystallized. For example, a bulk D_{Rb} value of 0.46 is calculated using the average partition coefficients for dacites and rhyolites reported in Henderson (1982) and assuming a mode of 10% biotite, 15% alkali feldspar, 20% plagioclase, 10% amphibole, 20% pyroxene, and 25% quartz (the D_{Rb} -value for amphibole used the average

for andesites because there is no value for rhyolites; quartz was assumed to have a D value of 0). Using these conservative bulk- D_{Rb} values and high $\Delta^{56}\text{Fe}_{\text{min-melt}}$ fractionation factors, however, would require $\sim 99\%$ crystallization to explain the high-Rb, high- $\delta^{56}\text{Fe}$ samples from Coso (Fig. 9); we cannot rule this out, but such extents of fractionation seem quite high. Moreover, we note that several of the high- $\delta^{56}\text{Fe}$, moderate Rb content Questa granitoids cannot be explained by Rayleigh fractionation using the parameters above (Fig. 7).

5.3. Trace-element tests of crystal fractionation

The similar charge/radius ratios of several trace elements provide a test of crystal fractionation mechanisms for explaining the $\delta^{56}\text{Fe}$ -composition trends observed in igneous rocks. Ratios of Zr/Hf are generally invariant relative to the chondritic ratio during crystal fractionation, but may be significantly changed during fluid–magma or fluid–rock interactions (e.g., Bau, 1996). The range in Zr/Hf ratios in igneous rocks that is considered to reflect mineral-melt partitioning due to charge and radius varies from ~ 26 to ~ 46 (defined as “Charac” or Charge and Radius Controlled behavior; Bau, 1996). Irber (1999) noted that the average Zr/Hf ratio for granites is 39, similar to the Chondrite average of 38. In contrast, high-silica igneous rocks often have low, “non-Charac” Zr/Hf ratios (Bau, 1996; Irber, 1999; Jahn et al., 2001; Veksler et al., 2005). Bau (1996) considered that the anomalous behavior shown by Zr and Hf reflects chemical complexation by elements such as F, Cl, B, Li, P, and CO_2 that are abundant in fluids derived from highly evolved magmas. Most authors consider the fractionation of Zr and Hf to be characteristic of highly differentiated magmatic melts, reflecting partitioning between silicate melts and depolymerized halogen-rich fluids during open-system evolution (e.g., Bau, 1996; Irber, 1999; Jahn et al., 2001; Veksler et al., 2005; Boulvais et al., 2006; Badanina et al., 2006). Some authors, however, consider fractional crystallization of accessory minerals that incorporate Zr and Hf, such as zircon, monazite, xenotime, and garnet, as an explanation for the observed fractionations (Linnen and Keppler, 2002), although such interpretations have been challenged (Veksler et al., 2006). Based on the very close charge/ionic radii ratios in this element pair, theories that are more sophisticated should be called upon to explain the observations. Fractionation of trace phases that contain Zr and Hf would not affect Fe isotope compositions if their Fe contents are low (e.g., zircon, monazite, xenotime, and apatite) or if they are rare in most magmas (garnet). Of the Fe-bearing phases that can incorporate Zr and Hf, ilmenite and magnetite are the only common phases that are liquidus minerals over a wide range of magmatic compositions, including high-silica systems. Both magnetite and ilmenite have near-chondritic Zr/Hf ratios (Bea et al., 2006), and thus could not produce the trends observed in Fig. 8. Additionally, Fe silicates such as amphibole and pyroxene, which could fractionate Fe isotopes, have Zr/Hf ratios that are also lower than Charac compositions (Bea et al., 2006) and thus fractionation of these Fe silicates could not produce the trends in Zr/Hf and

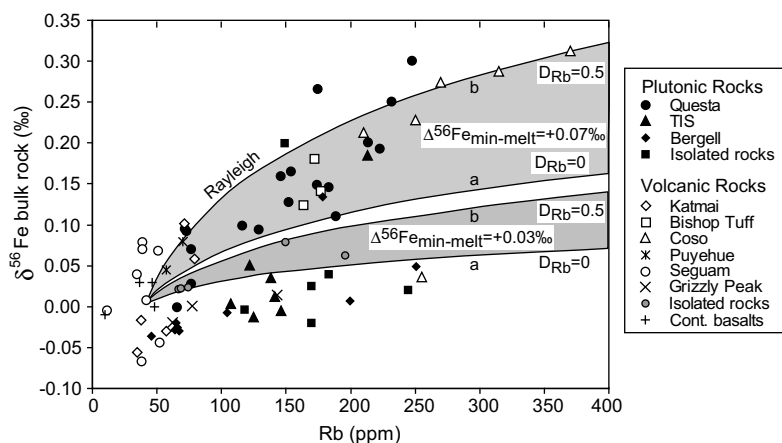


Fig. 7. Rayleigh fractionation models for bulk-rock Rb (ppm) and Fe isotopes ($\delta^{56}\text{Fe}$, ‰) as a function of temperature superimposed on a plot of measured bulk-rock $\delta^{56}\text{Fe}$ values versus Rb contents. The four curves were calculated combining the estimated mineral-melt Fe isotope fractionation factors shown in Fig. 6 ($\Delta^{56}\text{Fe}_{\text{min-melt}}$) at 900 and 700 °C of +0.03‰ and +0.07‰, respectively, with Rb mineral-melt distribution coefficients (D_{Rb}) of 0.0 and 0.5. The initial magma is assumed to have a $\delta^{56}\text{Fe}$ value of 0.0‰ and 40 ppm Rb. The curves labeled *a* and *b* reach up to 90% and 99% crystallization, respectively. References for data in [Electronic Annex Table EA-1](#).

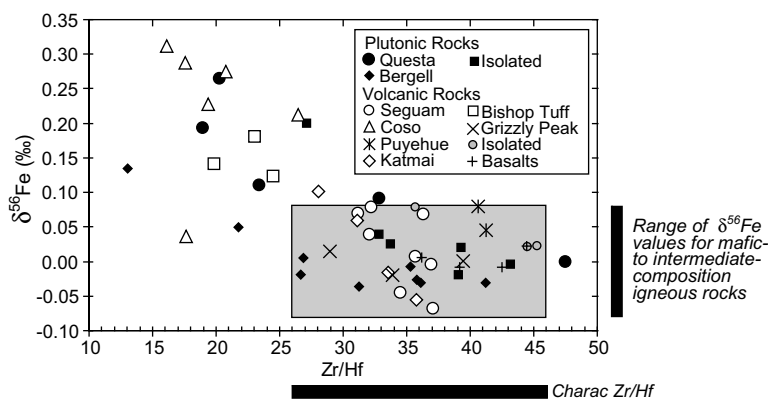


Fig. 8. Bulk-rock Zr/Hf ratios versus bulk-rock $\delta^{56}\text{Fe}$ values (‰) for the studied rocks for which Zr and Hf contents were available except for samples from the Bishop Tuff (which are those of similar rocks; see [Electronic Annex Table EA-1](#)). References for data in [Electronic Annex Table EA-1](#). The Zr/Hf “Charac” field is from Bau (1996).

$\delta^{56}\text{Fe}$ values observed in Fig. 8. We therefore argue that the most likely origin of the correlation of low Zr/Hf ratios with high $\delta^{56}\text{Fe}$ values in the high-Si samples is fractionation caused by fluid exsolution.

Other trace-element ratios such as Th/Ce or La/Ta are less reliable indicators of fluid exsolution, primarily because they may be changed by fractionation of accessory phases such as monazite, apatite, zircon, titanite, and allanite. Although an inverse correlation is observed between Th/Ce ratios and Zr/Hf ratios for the samples studied for which Zr, Hf, rare-earth elements (REEs) and Th contents are available (Figure not shown), such correlations are merely permissive of fluid exsolution. Detailed studies of the Questa granitoids led Johnson et al. (1989) to conclude that REE variations were well explained by crystal fractionation of accessory minerals contained in the rocks.

The focus on the origin of anomalous trace-element ratios (e.g., Y/Ho and Zr/Hf) has largely been devoted to characterizing the F contents of magmatic and hydrothermal fluids, which is not likely to substantially increase the

solubility of Fe in fluids. However, we note that such fluids also tend to be rich in Cl, which can strongly complex Fe and affect the amount of Fe partitioned into a fluid phase (e.g., Krauskopf, 1957; Chou and Eugster, 1977; Simon et al., 2004).

Of the samples studied, volcanic and plutonic rocks that have Zr/Hf ratios that fall within the range defined by Charac behavior also have a restricted range in $\delta^{56}\text{Fe}$ values that lies within the range of mafic- and intermediate-composition igneous rocks (Fig. 8, Tables 1 and 3; Table EA-1). In contrast, virtually all of the igneous rocks that have $\delta^{56}\text{Fe} > +0.10\text{‰}$ have anomalously low Zr/Hf ratios relative to the Charac field (Fig. 8). These relations suggest that the low-Zr/Hf, high- $\delta^{56}\text{Fe}$ igneous rocks do not reflect crystal fractionation, but may instead reflect loss of a low- $\delta^{56}\text{Fe}$ component through volatile exsolution, based on the evidence that anomalous Zr/Hf and Y/Ho ratios reflect interaction between halogen-rich fluids and silicate melt in highly evolved magmatic systems (Bau, 1996; Irber, 1999; Jahn et al., 2001; Veksler et al., 2005, 2006).

5.4. Magmatic volatile loss

Highly evolved magmas often possess large amounts of dissolved volatiles (e.g., H₂O, F, Cl, B, CO₂, and S) that are prone to unmixing when saturation conditions arise at decreasing temperatures prior to and during crystallization, eruption, and solidification (e.g., Wallace et al., 1995; Webster, 2004; Davidson and Kamenetsky, 2007). Transition-metal phases, including Fe, have been well documented inside bubbles within melt inclusions in volcanic rocks, indicating that metals can be preferentially partitioned into the volatile phase during crystallization and degassing (Lowenstern, 1993; Kamenetsky et al., 2002; Davidson and Kamenetsky, 2007). In addition, experimental studies of Fe transport have shown that Fe can be effectively mobilized into the volatile phase by saline chloride solutions (e.g., Chou and Eugster, 1977; Simon et al., 2004). Detailed studies of volatiles in melt inclusions are available for the Katmai, Bishop Tuff, and Coso volcanic suites studied here (Table 2).

Relations among eruption temperature, volatile contents, bulk-rock composition, and Fe isotope compositions for the Coso, Bishop Tuff, and Katmai samples indicate general correlations between the degree of differentiation, the extent of volatile loss, temperature of crystallization, and shifts in whole-rock $\delta^{56}\text{Fe}$ values (Fig. 9). We cast these relations relative to Cl/F ratios measured in melt inclusions and in bulk rocks. The melt inclusion data provide a window into the magma composition prior to eruption and solidification, whereas the bulk-rock composition is representative of post eruption. Crystal fractionation typically leaves Cl/F ratios unchanged or slightly increased (Macdonald et al., 1992). We therefore interpret the lower Cl/F ratios of melt inclusions and bulk rocks for Bishop Tuff and Coso relative to Katmai to indicate a larger degree of volatile loss and preferential partitioning of Cl into vapor relative to F. Fig. 9A plots the range of Cl/F ratios measured in melt inclusions and bulk rocks with the range of $\delta^{56}\text{Fe}$ values measured in bulk rocks for samples from Katmai and the Bishop Tuff because Fe isotope compositions were not determined on the same samples analyzed for Cl/F ratios (Table 2; Macdonald et al., 1992; Westrich et al., 1991; Wallace et al., 1999; Manley and Bacon, 2000). Coso melt inclusions have not been analyzed for Cl and F concentrations but we infer that the very low whole-rock Cl/F ratios reflect extensive Cl loss during late-stage crystallization and/or eruption (Fig. 9). That the lowest Cl/F ratios are measured for the most evolved (high Rb) rocks is expected because such rocks should have reached the highest total volatile contents and Cl is preferentially lost compared to F. This suggests that the high-Rb samples lost the greatest amount of volatiles, specifically Cl, which is consistent with the relatively low crystallization temperatures of the high-Rb samples (Tables 1 and 2).

Solubility relations for high-temperature ferrous chloride fluids indicate that magnetite solubility will control the extent of Fe-chloride exsolution from magmas (e.g., Chou and Eugster, 1977; Whitney et al., 1985; Simon et al., 2004). We suggest, therefore, that the positive magnetite–FeCl₄²⁻ Fe isotope fractionation factor (Fig. 6)

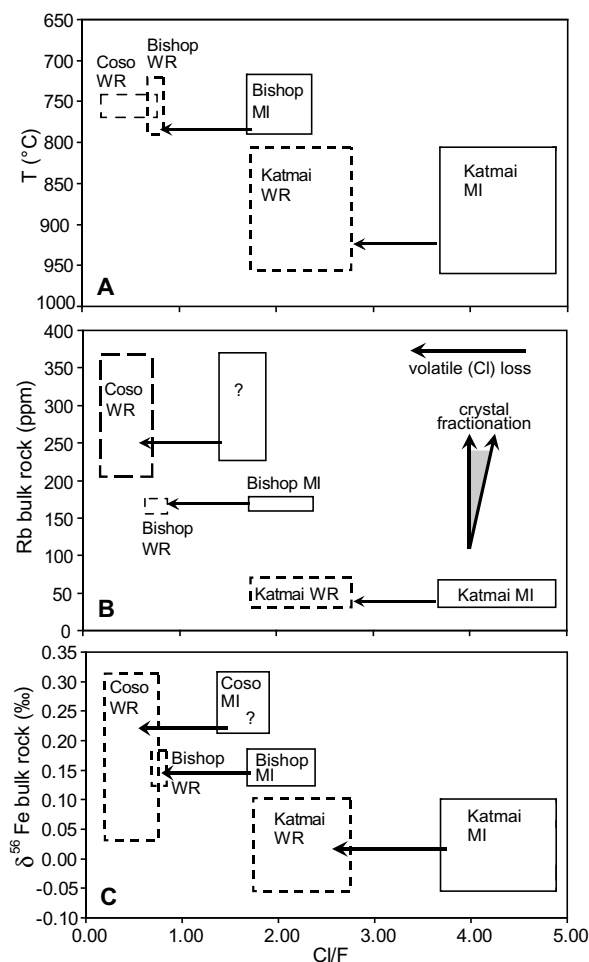


Fig. 9. Cl/F ratios from melt inclusions (MI, continuous lines) and whole rock (WR, dashed lines) for Katmai, Bishop Tuff, and Coso versus: (A) temperature (°C), (B) bulk-rock Rb (ppm), and (C) bulk-rock $\delta^{56}\text{Fe}$ (‰). Cl/F ratios and temperatures are shown as boxes and represent the minimum and maximum for rocks of similar composition as the ones analyzed for Fe isotopes. Chlorine and F MI contents for Coso are only a minimum estimate (Manley and Bacon, 2000) and are shown with a question mark in (B) and (C). Although MI Cl and F contents are not available for Coso samples, chemically they are similar in major and trace-element compositions to early-erupted Bishop Tuff high-silica rhyolites (Hildreth, 1979; Bacon et al., 1981), which gives an indication of the amount of Cl and F that may have been in the pre-eruptive magma. The trends expected during crystal fractionation are shown by arrows on Fig. 9B. The pre-eruptive Cl loss inferred from the difference between Cl/F in melt inclusion and bulk rock is also expressed by arrows. The length of the arrows does not indicate the extent of volatile loss. Volatile loss is inferred to be higher for Coso and Bishop Tuff compared to Katmai based on the correlation between smaller Cl/F ratios with lower crystallization temperatures and higher Rb contents in the former two. Melt inclusions for Coso and Bishop Tuff are considered to be more evolved than those for Katmai based on Rb contents in melt inclusions, and the magma had originally higher Cl/F ratios than when they were trapped. Melt inclusion Cl and F data taken from Westrich et al. (1991), Macdonald et al. (1992), Wallace et al. (1999), and Manley and Bacon (2000). Bulk-rock F and Cl data are from the same sources as in Fig. 1 and Tables 1 and 2. Temperatures are from the same sources as in Fig. 6 and Tables 1 and 2.

at magmatic temperatures predicts that an exsolved Fe-chloride fluid will have negative $\delta^{56}\text{Fe}$ values, which should produce relatively high $\delta^{56}\text{Fe}$ values in the remaining silicate melt and minerals. Qualitatively, the effect of Fe chloride exsolution is expected to be greatest in the most evolved magmas because such magmas reflect the greatest amount of Cl loss. Moreover, the lower temperatures of evolved magmas will involve the largest Fe isotope fractionations, and evolved rocks will have lower Fe contents and thus be more sensitive to changes in Fe isotope composition upon volatile/fluid exsolution.

Although crystal fractionation of less evolved precursor magmas was likely important in producing high volatile contents, we do not interpret crystal fractionation in the sense of crystal-melt segregation as the mechanism for producing high $\delta^{56}\text{Fe}$ values in evolved magmas. Our model of Fe-chloride fluid loss relies on the solubility of magnetite in equilibrium with such solutions, which in turn predicts that magnetite should record the greatest increases in $\delta^{56}\text{Fe}$ values upon volatile exsolution. This can be tested through detailed consideration of magnetite and Fe silicates in plutonic rocks that exsolved fluids during sub-solidus cooling at low temperatures where the isotopic fractionations are large, and this is discussed in the next section.

5.5. Fe isotope fractionation in plutonic rocks during sub-solidus fluid/rock interaction

Considerations of theoretical Fe isotope fractionation factors and magnetite solubility experiments suggest that the extent of Fe isotope fractionation during sub-solidus interaction between a plutonic rock and an exsolved fluid will largely be controlled by (1) the Cl content of the fluid, (2) the Fe content of the rock or magma, (3) the ratio of magnetite to Fe silicate minerals, and (4) the temperature of fluid exsolution. The most important external variables are temperature and HCl contents in the fluid (i.e., availability of ligands), and these variables are used in the model below. Pressure and $f\text{H}_2$ conditions will probably also influence Fe mobility and transport. Experimental studies indicate that Fe concentration in the volatile phase will tend to increase at higher pressures (e.g., Simon et al., 2004). Because oxygen fugacity was fixed to the hematite–magnetite buffer at 400–600 °C and 1–2 kbar pressure in the experiments of Chou and Eugster (1977) and Boctor et al. (1980) in which Fe existed in the form of ferrous chloride (FeCl_2^0), a more relevant variable is $f\text{H}_2$. Qualitatively, relatively high $f\text{H}_2$ (or low $f\text{O}_2$) conditions will tend to favor Fe^{2+} mobilization in solution, whereas high- $f\text{O}_2$ conditions will tend to deposit Fe (e.g., Eugster, 1986). To our knowledge, however, no experimental results have been published on the effects of changing $f\text{O}_2$ conditions on Fe solubility. The effects of these variables on Fe isotope fractionation factors have not been investigated in experiments.

The absence of a correlation between bulk-rock $\delta^{18}\text{O}$ values (Table 1; Johnson et al., 1990; Lackey, 2005) and $\delta^{56}\text{Fe}$ values for the plutonic rocks studied here suggests that circulation of Cl-poor meteoric fluids did not affect the Fe isotope compositions of Questa or TIS granitoids. In contrast, rocks from Questa that underwent high-tem-

perature alteration and contain Mo mineralization (Johnson et al., 1990), as well as a sample from the Johnson Granite Porphyry (TIS), have high $\delta^{56}\text{Fe}$ values, suggesting that Cl-rich high-temperature fluids affected the Fe isotope composition of the rocks. The Johnson Granite Porphyry is the last and innermost unit of the TIS and is thought to represent a partially erupted magma, as indicated by miarolitic cavities and evidence of fluid exsolution (Bateman and Chappell, 1979; Lackey, 2005). These observations are in agreement with the high $\delta^{56}\text{Fe}$ values of the Johnson Granite Porphyry, compared to the near-zero $\delta^{56}\text{Fe}$ values of all the other rocks from the TIS. Sub-solidus re-equilibration temperatures for Questa Granitoids and TIS are similar (Table 1), which suggests that the granitoids from TIS that have “normal” $\delta^{56}\text{Fe}$ values contained relatively low fluid contents or did not exsolve significant amounts of fluids. Moreover, the higher crystallization temperatures and Fe contents of the TIS units that lie outboard of the Johnson Granite Porphyry would minimize any shift in $\delta^{56}\text{Fe}$ values upon fluid exsolution. It is noteworthy that a positive correlation between $\delta^{18}\text{O}$ and $\delta^{56}\text{Fe}$ values in the Bergell intrusion was explained by crystal fractionation or assimilation of high- $\delta^{56}\text{Fe}$, high- $\delta^{18}\text{O}$ crustal material, although the last proposal requires the presence of high- $\delta^{56}\text{Fe}$ sedimentary rocks, which are rare (Schoenberg and von Blanckenburg, 2006).

The solubility experiments of Chou and Eugster (1977) show that considerable amounts of Fe can be present in a chloride-rich fluid (0.24–16.4 wt.% Fe at 700–500 °C; Fig. 10) as FeCl_2^0 in equilibrium with magnetite. The rapidly increasing solubility with decreasing temperature (Fig. 10) indicates that loss of Fe through fluid exsolution will be greatest at lower temperatures where the Fe isotope fractionations are largest, consistent with the positive $\delta^{56}\text{Fe}$ values observed in the lowest-temperature or most evolved samples. The range in Fe contents measured in the

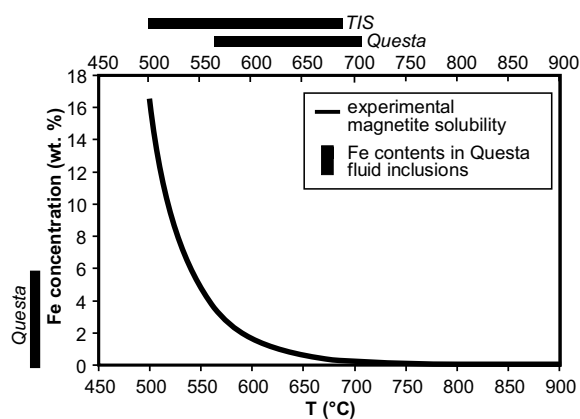


Fig. 10. Concentration of Fe (wt.%, as FeCl_2^0 species) in a Cl-bearing fluid as a function of temperature (°C). The curve is based on magnetite dissolution experiments (Chou and Eugster, 1977) and the black vertical box represents the ranges in Fe contents measured in fluid inclusions from Questa granitoids (Audétat and Pettke, 2003). The top bars represent temperatures for Questa and TIS granitoids (as in Fig. 6).

solubility experiments is supported by fluid inclusion data on natural samples. Fluid inclusions from the same Questa granitoids studied here contain high amounts of Cl (up to 40 wt.% NaCl_{equiv}) and Fe (0.16–5.7 wt.% Fe; Audétat and Pettke, 2003), indicating that significant amounts of Fe were present in a late-stage, Cl-bearing fluid phase. The high $\delta^{56}\text{Fe}$ values of magnetite and the positive correlation between $\Delta^{56}\text{Fe}_{\text{Mgt-Bt}}$ and bulk-rock $\delta^{56}\text{Fe}$ (Figs. 4 and 5) suggest that magnetite re-equilibration took place at sub-solidus conditions and this process is modeled below.

5.5.1. Model construction

The Fe isotope exchange during cooling between a rock and an exsolved chloride-bearing fluid was modeled from 700 to 500 °C using mass-balance equations, the modal abundances of magnetite and Fe silicates in the studied rocks from Questa, fluid volumes that are typical of siliceous granitic magmas (5–10 wt.% fluid), and Fe isotope fractionation factors that have been calculated from theory. The Fe isotope mass balance of a system composed of magnetite, biotite, and fluid is defined by:

$$\delta^{56}\text{Fe}_{\text{system}} = \delta^{56}\text{Fe}_{\text{magnetite}} \cdot X_{\text{Mgt}}^{\text{Fe}} + \delta^{56}\text{Fe}_{\text{biotite}} \cdot X_{\text{Bt}}^{\text{Fe}} + \delta^{56}\text{Fe}_{\text{fluid}} \cdot X_{\text{fl}}^{\text{Fe}}, \quad (4)$$

where $X_{\text{Mgt}}^{\text{Fe}}$, $X_{\text{Bt}}^{\text{Fe}}$, and $X_{\text{fl}}^{\text{Fe}}$ are the Fe molar proportions of magnetite, biotite, and fluid, respectively. The initial system is defined to have a $\delta^{56}\text{Fe}$ value of 0.00‰ at 700 °C. The calculation was performed at other temperatures and assumed that the total amount of Fe in the system was constant but that Fe contents and $\delta^{56}\text{Fe}$ values for biotite, the fluid, and magnetite varied from 700 to 500 °C based on changing solubility of Fe in the fluid using the experimental work of Chou and Eugster (1977). Iron contents in biotite remain unchanged. Iron concentrations in the fluid were calculated at different temperatures after rearranging the solubility equation of Chou and Eugster (1977):

$$\log m\text{FeCl}_2 = [6887.0/T \text{ (K)}] - 8.44, \quad (5)$$

to

$$m\text{Fe}_{\text{fl}}^T = 3 \cdot 10^{35} \cdot T^{-12.698}, \quad (6)$$

where m is the mass of Fe in the fluid calculated from the concentration of Fe in the fluid in wt.% normalized to the amount of fluid in the system, and T is the temperature in °C (see Fig. 10). The mass of Fe in magnetite ($m\text{Fe}_{\text{Mgt}}$) was first calculated at the lowest temperature (500 °C) from the current modal proportion of magnetite in the rock, based on the assumption that the modal proportions of the Fe-bearing minerals were “locked in” at the quartz–magnetite oxygen isotope closure temperatures (~ 500 °C). The mass of Fe in biotite was calculated in the same way and was assumed to be constant. The mass of Fe in magnetite at higher temperatures was calculated by subtracting the mass of Fe in the fluid ($m\text{Fe}_{\text{fl}}^T$) and biotite ($m\text{Fe}_{\text{Bt}}^T$) from the amount of Fe in the system ($m\text{Fe}_{\text{system}}$):

$$m\text{Fe}_{\text{Mgt}}^T = m\text{Fe}_{\text{system}} - m\text{Fe}_{\text{fl}}^T - m\text{Fe}_{\text{Bt}}^T, \quad (7)$$

where the superscript T indicates the increment calculation performed at a specific temperature. Iron molar propor-

tions for each phase were calculated by normalizing to the total amount of Fe in the system; for magnetite this is:

$$X_{\text{Mgt}}^{\text{Fe}} = m\text{Fe}_{\text{Mgt}}/m\text{Fe}_{\text{system}} = m\text{Fe}_{\text{Mgt}}/(m\text{Fe}_{\text{Mgt}} + m\text{Fe}_{\text{fl}} + m\text{Fe}_{\text{Bt}}). \quad (8)$$

Iron molar fractions for biotite and the fluid were calculated in the same way (Fig. 11). The molar fraction of Fe in magnetite decreases as that of the fluid increases from 700 to 500 °C. The $\delta^{56}\text{Fe}$ values for magnetite, biotite, the fluid, and bulk rock were calculated as a function of temperature using the Fe isotope fractionation factors from Polyakov and Mineev (2000), Schauble et al. (2001), and Polyakov et al. (2007), and rearranging Eq. (4) to:

$$\delta^{56}\text{Fe}_{\text{Mgt}} = X_{\text{Bt}}^{\text{Fe}} \cdot \Delta_{\text{Mgt-Fe sil}} + X_{\text{fl}}^{\text{Fe}} \cdot \Delta_{\text{Mgt-fl}}, \quad (9)$$

$$\delta^{56}\text{Fe}_{\text{Bt}} = \delta^{56}\text{Fe}_{\text{Mgt}} - \Delta_{\text{Mgt-Fe sil}}, \quad (10)$$

$$\delta^{56}\text{Fe}_{\text{fluid}} = \delta^{56}\text{Fe}_{\text{Mgt}} - \Delta_{\text{Mgt-fl}}, \quad \text{and} \quad (11)$$

$$\delta^{56}\text{Fe}_{\text{rock}} = [\delta^{56}\text{Fe}_{\text{Mgt}} \cdot X_{\text{Mgt}}^{\text{Fe}} / (X_{\text{Mgt}}^{\text{Fe}} + X_{\text{Bt}}^{\text{Fe}})] + [\delta^{56}\text{Fe}_{\text{Bt}} \cdot X_{\text{Bt}}^{\text{Fe}} / (X_{\text{Bt}}^{\text{Fe}} + X_{\text{Mgt}}^{\text{Fe}})]. \quad (12)$$

5.5.2. Prediction of $\delta^{56}\text{Fe}$ values of magnetite, Fe silicates, bulk rocks, and exsolved fluid

Based on the constructed model, magnetite is expected to have positive $\delta^{56}\text{Fe}$ values, whereas biotite and the fluid will have slightly negative values (Fig. 12). The model predicts that the $\delta^{56}\text{Fe}$ values of magnetite in equilibrium with an Fe chloride-bearing fluid and biotite will become progressively higher ($\delta^{56}\text{Fe}$ up to +0.4‰) as temperature decreases from 700 to 500 °C (Figs. 12 and 13). The $\delta^{56}\text{Fe}$ values for the fluid range from -0.39 ‰ to -0.05 ‰.

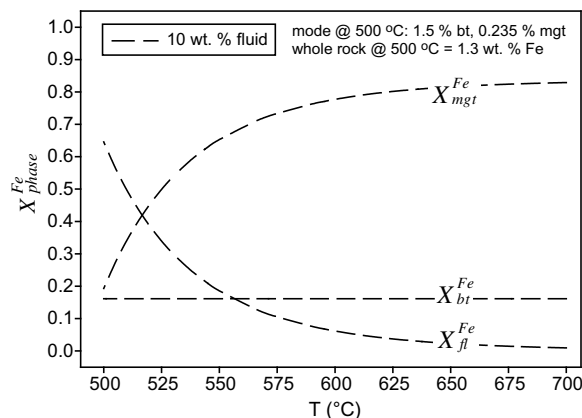


Fig. 11. Calculated Fe molar fractions ($X_{\text{phase}}^{\text{Fe}}$) for magnetite, biotite, and fluid as a function of temperature (700–500 °C) for a granitic rock in equilibrium with 10 wt.% of exsolved Cl-bearing fluid phase. Iron in the fluid is derived from the dissolution of magnetite and calculated from the experimental equation of Chou and Eugster (1977). At 500 °C the rock contains 1.5% modal biotite, 0.235% modal magnetite, and 1.3% Fe, which corresponds to ($X_{\text{phase}}^{\text{Fe}}$) values for biotite:magnetite:fluid of 0.19:0.16:0.65. The modal abundance of Fe silicates in the studied granites ranges from 1% to 3% (Johnson et al., 1990). Total Fe in the rock was chosen at 1.3 wt.% because it is typical for the studied rocks. End-member magnetite was used in the calculations.

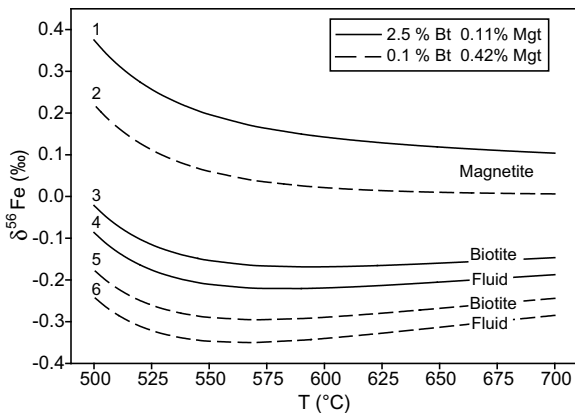


Fig. 12. Modeled $\delta^{56}\text{Fe}$ (‰) values for magnetite, biotite, and fluid for the interaction of a rock and 10 wt.% of exsolved Cl-bearing fluid as a function of temperature from 700 to 500 °C. Curves represent two modal abundances of magnetite and biotite for which most Fe is hosted in magnetite or biotite and that represent extreme magnetite and biotite contents for similar granitoid rocks. Solid lines correspond to $\delta^{56}\text{Fe}$ values of a reacted rock that has a final modal abundance at 500 °C of 2.5% biotite and 0.11% magnetite and molar fractions of Fe in magnetite:biotite:fluid of 0.09:0.27:0.65. Dashed lines represent $\delta^{56}\text{Fe}$ values for a modal abundance of biotite and magnetite at 500 °C of 0.1% and 0.42%, respectively, and molar Fe fractions of magnetite:biotite:fluid of 0.34:0.01:0.65. The $\delta^{56}\text{Fe}$ value for the total Fe in the system is 0‰. Details of the calculation for the $\delta^{56}\text{Fe}$ values and Fe concentrations in minerals and fluids are presented in the text.

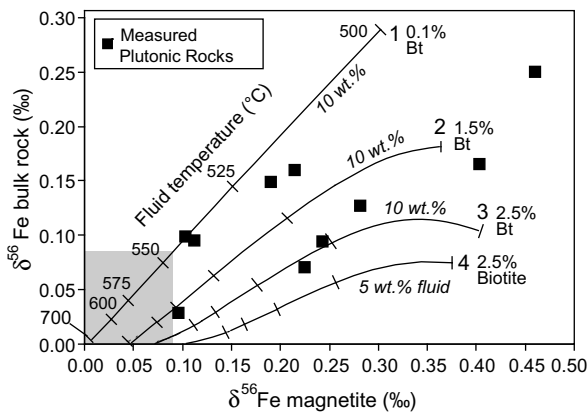


Fig. 13. Modeled $\delta^{56}\text{Fe}$ (‰) values for magnetite and its bulk rock that result from the down-temperature interaction of a crystallizing granitoid with 10 wt.% (curves 1–3) and 5 wt.% (curve 4) exsolved fluid phase. Each curve represents a rock with the same Fe content (1.3 wt.%) and different magnetite and biotite (mgt, bt) modal abundances at 500 °C as follows: (1) 0.1% bt, 0.416% mgt; (2) 1.5% bt, 0.235% mgt; (3) 2.5% bt, 0.105% mgt; (4) 2.5% bt, 0.105% mgt. Iron molar fractions for these modal abundances for magnetite:biotite:fluid are: (1) 0.34:0.01:0.65; (2) 0.19:0.16:0.65; (3) 0.09:0.27:0.65; and (4) 0.13:0.41:0.46. Tick marks represent temperature (°C) starting from 700 °C and ending at 500 °C. Shown as squares are measured bulk-rock and magnetite compositions for Questa granitoids. The shaded field represents the mean and 2 standard deviation error $\delta^{56}\text{Fe}$ value of crustal mafic- to intermediate-composition igneous rocks.

Removal of the low- $\delta^{56}\text{Fe}$ fluid through volatile loss will produce an increase in the $\delta^{56}\text{Fe}$ values of the remaining rock, and this increase will be greatest at the lowest temperatures (Fig. 13). Measured $\delta^{56}\text{Fe}$ values for magnetite and bulk rock from Questa granitoids fall within the values predicted by the model (Fig. 13). The increase in $\delta^{56}\text{Fe}$ values of the bulk rock is greatest when the magnetite/Fe silicate Fe molar ratio is the highest (curves 1 and 2; $\delta^{56}\text{Fe}$ up to $\sim +0.30$ ‰), reflecting the importance of magnetite abundance on the Fe content of the fluid, and the relatively large magnetite–silicate and magnetite–Fe chloride fractionation factors. As expected, bulk-rock $\delta^{56}\text{Fe}$ values will be highest when large amounts of fluid are exsolved (Fig. 13, curves 3 and 4, 10 and 5 wt.% fluid, respectively).

5.6. The Fe isotope composition of the Earth's crust

The Fe isotope composition of the Earth's crust based on mafic- to intermediate-composition igneous rocks is extremely homogeneous ($\delta^{56}\text{Fe} = 0.00 \pm 0.08$ ‰, 2-SD; Fig. 2). This isotopic homogeneity is extended to sedimentary rocks that have not undergone extensive anoxic diagenesis (e.g., Beard et al., 2003b), and this, in turn, provides a powerful reference frame for interpreting the origin of Fe isotope fractionations (Beard and Johnson, 2004; Johnson and Beard, 2006b; Johnson et al., 2008). The occurrence of high $\delta^{56}\text{Fe}$ values in some igneous rocks has led some researchers to question the validity of using the Earth's crust as a reference reservoir (e.g., Poitras and Frey, 2005). If the total Fe budget of the crust is considered, however, the contribution of Fe from Fe-poor, high-silica igneous rocks represents only a small fraction of the crustal Fe inventory (Fig. 14), a point discussed by

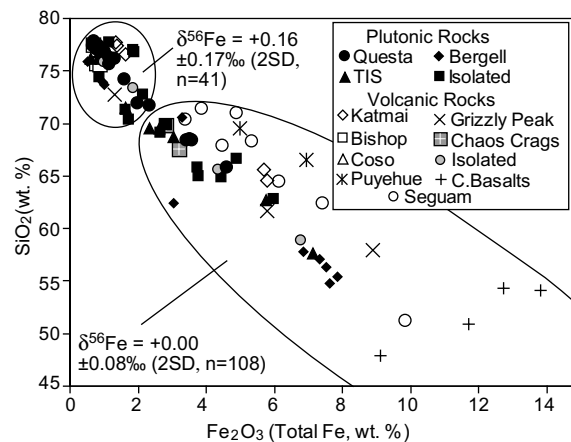


Fig. 14. Bulk-rock Fe_2O_3 (wt.%, total Fe) versus SiO_2 (wt.%) for the studied rocks and data taken from the literature (from same sources as in previous Figures). High-silica igneous rocks represent a small proportion of the total Fe budget of the Earth's crust. The average $\delta^{56}\text{Fe}$ value of rocks that have <70 wt.% SiO_2 and >2 wt.% Fe_2O_3 (including basalts, andesites, granitoids, and acid volcanic rocks) is 0.00 ± 0.08 ‰ (2 standard deviation error (2-SD), $n = 108$), whereas that of igneous rocks with >70 wt.% SiO_2 and <2 wt.% Fe_2O_3 is $+0.16 \pm 0.17$ ‰ (2-SD, $n = 41$). The averages were calculated with data reported in Electronic Annex Tables EA-1 and EA-2 and data for basalts referenced in Fig. 2.

Beard and Johnson (2006) and Poitrasson (2006). Moreover, high $\delta^{56}\text{Fe}$ values are not a uniform characterization of evolved igneous rocks, but instead are produced only in those systems that developed high volatile contents, specifically rich in chloride, which subsequently lost volatiles by fluid exsolution. Based on the low solubility of Fe in F-rich fluids, magmatic systems that have high F/Cl ratios are not expected to have unusual Fe isotope compositions. The inventory of Fe in the crust that is cycled through this process is very small, probably much less than 1%, indicating that to an excellent approximation, the average $\delta^{56}\text{Fe}$ value of the crust lies near zero on the igneous rock scale of Beard et al. (2003a). This implies that the concentration-weighted Fe isotope composition of Fe that is delivered to the sedimentary system also lies very close to $\delta^{56}\text{Fe} = 0\text{‰}$.

6. CONCLUSIONS AND FUTURE DIRECTIONS

High-silica igneous rocks may have $\delta^{56}\text{Fe}$ values up to $+0.30\text{‰}$, significantly higher than those of mafic- to intermediate-composition igneous rocks, which have a restricted range of $\delta^{56}\text{Fe} = 0.00 \pm 0.08\text{‰}$ (2-SD). Not all high-silica igneous rocks, however, have high $\delta^{56}\text{Fe}$ values. Igneous rocks with high $\delta^{56}\text{Fe}$ values appear to be restricted to highly evolved rocks that contain evidence for loss of Fe chloride fluids based on volatile contents and anomalous trace-element ratios. The isotopic effects of fluid loss are most pronounced in evolved, low-Fe content rocks that lost Cl-bearing fluids at low magmatic or sub-solidus temperatures. A positive correlation between the magnetite–Fe silicate fractionation and bulk-rock $\delta^{56}\text{Fe}$ values in mineralized granitoids indicates that the rocks underwent open-system Fe isotope exchange and fluid loss. Multiple lines of evidence indicate that high- $\delta^{56}\text{Fe}$ igneous rocks are not likely to have formed through fractional crystallization but by complexation of Fe with Cl in volatile-rich, high-silica magmatic systems, followed by fluid loss. That the highest $\delta^{56}\text{Fe}$ values occur in samples that crystallized at the lowest temperatures or underwent sub-solidus fluid loss, as indicated by low oxygen isotope temperatures, is well explained by the relatively high solubility of magnetite at low temperatures and the large magnetite-fluid fractionations that occur at low temperatures. The hypothesis proposed here can be tested by analysis of magnetite and Fe silicate separates from the same rock, which are helpful for distinguishing processes responsible for Fe isotope fractionations, compared to bulk-rock Fe isotope compositions alone. Plots of fractionation factors against Fe isotope compositions of minerals and bulk rocks are useful indicators for high-temperature fractionation processes, as shown by numerous oxygen isotope studies in the 1980s, and for iron isotopes by recent studies (Beard and Johnson, 2004).

Our results have implications for transition-metal stable isotope studies of hydrothermal ore deposits. Fluids exsolved from siliceous hydrous magmas may represent precursors to mineralizing fluids that sometimes produce porphyry-style Cu or Cu–Au mineralization (e.g., Krauskopf, 1957; Kamenetsky et al., 2002; Halter and Heinrich, 2006). These types of deposits, as well as hydrothermal Fe deposits,

may have anomalous Fe isotope compositions (e.g., Graham et al., 2004; Markl et al., 2006), and our results suggest that superposition of hydrothermal events, including sub-solidus re-equilibration and precipitation of sulfides from a Cl-bearing fluid, may control the Fe isotope composition of such deposits. Because Fe solubility in F-rich fluids is low, we would not expect Fe isotope compositions of high-F/Cl magmatic/hydrothermal systems to significantly deviate from the average of igneous rocks. Because the transition metals are soluble in chloride-rich fluids, detailed studies of Fe (and possibly Cu and Zn) isotopes in ore deposits may provide a unique identification of magmatic fluid contribution to hydrothermal ore deposits. Future success of this application will depend upon high-temperature experimental studies of Fe isotope fractionation in fluid–melt and fluid–mineral systems, with particular attention paid to Fe–Cl speciation.

ACKNOWLEDGMENTS

We thank Charles Bacon, Wes Hildreth, Brian Jicha, and Jade Star Lackey for providing some of the samples used in this study. Brian Jicha provided unpublished Fe–Ti oxide temperatures for Se-guam Island rocks, Wes Hildreth provided unpublished Bishop Tuff and Katmai chemical compositions, and Jade Star Lackey provided oxygen isotope temperatures for TIS samples. Garret Hart, Peter Hooper, and Frank Tepley are thanked for providing compositional data. Discussions with Charles Bacon, Phil Brown, Wes Hildreth, Dima Kamenetsky, Jacob Lowenstern, Adam Simon, Brad Singer, and Paul Wallace helped focus this study. Morgan Herrick helped with Fe isotope analyses. We also thank Associate Editor Dr. E. Ripley and two reviewers, Drs. H. Williams and M. Sharma, for their constructive suggestions. This study was supported by NSF Grant EAR-0318213 to C.M.J.

APPENDIX A. SUPPLEMENTARY DATA

Supplementary data associated with this article can be found, in the online version, at [doi:10.1016/j.gca.2008.06.009](https://doi.org/10.1016/j.gca.2008.06.009).

REFERENCES

- Albarède F. and Beard B. L. (2004) Analytical methods for non-traditional stable isotopes. In *Geochemistry of Non-traditional Stable Isotopes*, vol. 55 (eds. C. M. Johnson, B. L. Beard and F. Albarède). *Rev. Mineral. Geochem.*, pp. 113–152.
- Audétat A. and Pettke T. (2003) The magmatic-hydrothermal evolution of two barren granites: a melt and fluid inclusion study of the Rito del Medio and Cañada Pinabete plutons in northern New Mexico (USA). *Geochim. Cosmochim. Acta* **67**(1), 97–121.
- Bacon C. R., Macdonald R., Smith R. L. and Baedeker P. A. (1981) Pleistocene high-silica rhyolites of the Coso volcanic field, Inyo County, California. *J. Geophys. Res.* **86**(B11), 10223–10241.
- Badanina E. V., Trumbull R. B., Dulski P., Wiedenbeck M., Veksler I. V. and Syritso L. F. (2006) The behavior of rare-earth and lithophile trace elements in rare-metal granites: a study of fluorite, melt inclusions and host rocks from the Khangilay Complex, Transbaikalia, Russia. *Can. Mineral.* **44**(3), 667–692.

- Bateman P. C. and Chappell B. W. (1979) Crystallization, fractionation, and solidification of the Tuolumne Intrusive Series, Yosemite National Park, California. *Geol. Soc. Am. Bull.* **90**, 465–482.
- Bau M. (1996) Controls on the fractionation of isovalent trace elements in magmatic and aqueous systems: evidence from Y/Ho, Zr/Hf, and lanthanide tetrad effect. *Contrib. Mineral. Petr.* **123**, 323–333.
- Bea F., Montero P. and Ortega M. (2006) A LA-ICP-MS evaluation of Zr reservoirs in common crustal rocks: implications for Zr and Hf geochemistry, and zircon-forming processes. *Can. Mineral.* **44**(3), 693–714.
- Beard B. L. and Glazner A. F. (1995) Trace element and Sr and Nd composition of mantle xenoliths from the Big Pine volcanic field, California. *J. Geophys. Res.* **100**(B3), 4169–4179.
- Beard B. L. and Johnson C. M. (1997) Hafnium isotope evidence for the origin of Cenozoic basaltic lavas from the southwestern United States. *J. Geophys. Res.* **102**(B9), 20149–20178.
- Beard B. L. and Johnson C. M. (2004) Inter-mineral Fe isotope variations in mantle-derived rocks and implications for the Fe geochemical cycle. *Geochim. Cosmochim. Acta* **68**, 4727–4743.
- Beard B. L. and Johnson C. M. (2006) Comment on “Heavy iron isotope composition of granites determined by high resolution MC-ICP-MS” by F. Poitrasson and R. Freydir [Chem. Geol. **222**, 132–147]. *Chem. Geol.* **235**, 201–204.
- Beard B. L., Johnson C. M., Skulan J. L., Nealon K. H., Cox L. and Sun H. (2003a) Application of Fe isotopes to tracing the geochemical and biological cycling of Fe. *Chem. Geol.* **195**, 87–117.
- Beard B. L., Johnson C. M., Von Damm K. L. and Poulson R. L. (2003b) Iron isotope constraints on Fe cycling and mass balance in oxygenated Earth oceans. *Geology* **31**, 629–632.
- Boctor N. Z., Popp R. K. and Frantz J. D. (1980) Mineral solution equilibria: IV. Solubilities and the thermodynamic properties of FeCl_2^0 in the system $\text{Fe}_2\text{O}_3\text{-H}_2\text{-H}_2\text{O-HCl}$. *Geochim. Cosmochim. Acta* **44**, 1509–1518.
- Boulvais P., Ruffet G., Cornichet J. and Mermet M. (2006) Cretaceous albitization and dequartzification of Hercynian peraluminous granite in the Salvezines Massif (French Pyrenees). *Lithos* **93**(1–2), 89–106.
- Chou I.-M. and Eugster H. P. (1977) Solubility of magnetite in supercritical chloride solutions. *Am. J. Sci.* **277**, 1296–1314.
- Clayton R. N. and Kieffer S. W. (1991) Oxygen isotopic thermometer calibrations. In *Stable Isotope Geochemistry: A Tribute to Samuel Epstein*, 3 (eds. H. P. Taylor, J. R. O’Neil and I. R. Kaplan). Geochemical Society Special Publication, pp. 3–10.
- Dauphas N. and Rouxel O. (2006) Mass spectrometry and natural variations of iron isotopes. *Mass Spectrom. Rev.* **25**, 515–550.
- Dauphas N., van Zuilen M., Wadhwa M., Davis A. M., Marty B. and Janney P. E. (2004) Clues from Fe isotope variations on the origin of early Archean BIFs from Greenland. *Science* **306**, 2077–2080.
- Davidson P. and Kamenetsky V. S. (2007) Primary aqueous fluids in rhyolitic magmas: melt inclusion evidence for pre- and post-trapping exsolution. *Chem. Geol.* **237**, 372–383.
- Deer W. A., Howie R. A. and Zussman J. (1992) *An Introduction to Rock-Forming Minerals*. Prentice Hall.
- Eugster H. P. (1986) Minerals in hot water. *Am. Mineral.* **71**, 655–673.
- Fridrich C. J. (1987) The Grizzly Peak cauldron, Colorado: structure and petrology of a deeply dissected resurgent ash-flow caldera. Ph.D. Thesis, Stanford University.
- Gerlach D. G., Frey F. A., Moreno-Roa H. and Lopez-Escobar L. (1988) Recent volcanism in the Puyehue-Cordon Caulle region, southern Andes, Chile (40.5°S): petrogenesis of evolved lavas. *J. Petrol.* **29**(2), 333–382.
- Ghiorso M. S. and Sack R. O. (1995) Chemical mass transfer in magmatic processes: IV. A revised and internally consistent thermodynamic model for the interpolation and extrapolation of liquid-solid equilibria in magmatic systems at elevated temperatures and pressures. *Contrib. Mineral. Petrol.* **119**(2–3), 197–212.
- Graham S., Pearson N., Jackson S., Griffin W. and O’Reilly S. Y. (2004) Tracing Cu and Fe from source to porphyry: in situ determination of Cu and Fe isotope ratios in sulfides from the Grasberg Cu–Au deposit. *Chem. Geol.* **207**, 147–169.
- Hagstrum J. T. and Johnson C. M. (1986) A paleomagnetic and stable isotope study of the pluton at Rio Hondo near Questa, New Mexico: implications for CRM related to hydrothermal alteration. *Earth Planet. Sci. Lett.* **78**, 296–314.
- Halter W. E. and Heinrich C. A. (2006) Magmatic processes and volatile phase generation in porphyry-type environments: a laser ablation-ICP-MS study of silicate and sulfide melt inclusions. In *Melt Inclusions in Plutonic Rocks*, vol. 36 (ed. J. D. Webster). Mineral. Assoc. Canada Short Course Series, pp. 151–164.
- Henderson P. (1982) *Inorganic Geochemistry*. Pergamon Press.
- Hildreth W. (1979) The Bishop Tuff: evidence for the origin of compositional zonation in silicic magma chambers. In *Ash-Flow Tuffs*, vol. 180 (eds. C. E. Chapin and W. E. Elston). Geol. Soc. Am. Spec. Pap., pp. 43–75.
- Hildreth W. (1983) The compositionally zoned eruption of 1912 in the Valley of Ten Thousand Smokes, Katmai National Park, Alaska. *J. Volcanol. Geoth. Res.* **18**, 1–56.
- Huang F., Lundstrom C. C. and Ianno A. J. (2007) Mg and Fe isotopes as tracers of temperature gradient driven diffusive differentiation. *Geochim. Cosmochim. Acta* **71**(15), A422.
- Irber W. (1999) The lanthanide tetrad effect and its correlation with K/Rb, Eu/Eu*, Sr/Eu, Y/Ho, and Zr/Hf of evolving peraluminous granite suites. *Geochim. Cosmochim. Acta* **63**(3/4), 489–508.
- Jahn B.-m., Wu F., Capdevila R., Martineau F., Zhao Z. and Wang Y. (2001) Highly evolved juvenile granites with tetrad REE patterns: the Woduhe and Baerzhe granites from the Great Xing’an Mountains in NE China. *Lithos* **59**, 171–198.
- Jicha B. R., Singer B. S., Beard B. L. and Johnson C. M. (2005) Contrasting timescales of crystallization and magma storage beneath the Aleutian Island arc. *Earth Planet. Sci. Lett.* **236**, 195–210.
- Jicha B. R., Singer B. S., Beard B. L., Johnson C. M., Roa H. M. and Naranjo J. A. (2007) Rapid magma ascent and generation of ^{230}Th excesses in the lower crust at Puyehue-Cordon Caulle, Southern Volcanic Zone, Chile. *Earth Planet. Sci. Lett.* **255**, 229–242.
- Johnson C. M. and Beard B. L. (2006a) Tracing metasomatic and crystallization processes in the mantle through Fe isotopes. *Geochim. Cosmochim. Acta* **70**(1), A295.
- Johnson C. M. and Fridrich C. J. (1990) Non-monotonic chemical and O, Sr, Nd, and Pb isotope zonations and heterogeneity in the mafic- to silicic-composition magma chamber of the Grizzly Peak Tuff, Colorado. *Contrib. Mineral. Petrol.* **105**, 677–690.
- Johnson C. M. and Beard B. L. (2006b) Fe isotopes: an emerging technique for understanding modern and ancient biogeochemical cycles. *GSA Today* **16**(11), 4–10.
- Johnson C. M., Czamanske G. K. and Lipman P. W. (1989) Geochemistry of intrusive rocks associated with the Latir volcanic field, New Mexico, and contrasts between evolution of plutonic and volcanic rocks. *Contrib. Mineral. Petrol.* **103**, 90–109.

- Johnson C. M., Lipman P. W. and Czamanske G. K. (1990) H, O, Sr, Nd, and Pb isotope geochemistry of the Latir volcanic field and cogenetic intrusions, New Mexico, and relations between evolution of a continental magmatic center and modifications of the lithosphere. *Contrib. Mineral. Petrol.* **104**, 99–124.
- Johnson C. M., Beard B. L. and Roden E. E. (2008) The iron isotope fingerprints of redox and biogeochemical cycling in the modern and ancient Earth. *Annu. Rev. Earth Planet. Sci.* **36**, 457–493.
- Kamenetsky V. S., Davidson P., Mernagh T. P., Crawford A. J., Gemmel J. V., Portnyagin M. V. and Shinjo R. (2002) Fluid bubbles in melt inclusions and pillow-rim glasses: high-temperature precursors to hydrothermal fluids? *Chem. Geol.* **183**, 349–364.
- Krauskopf K. B. (1957) The heavy metal content of magmatic vapor at 600 °C. *Econ. Geol.* **52**, 786–807.
- Lackey J. S. (2005) The magmatic and alteration history of the Sierra Nevada Batholith as recorded by oxygen isotope ratios of zircon, titanite, garnet, and quartz. Ph.D. Thesis, University of Wisconsin-Madison.
- Linnen R. L. and Keppler H. (2002) Melt composition control of Zr/Hf fractionation in magmatic processes. *Geochim. Cosmochim. Acta* **66**(18), 3293–3301.
- Lowenstern J. B. (1993) Evidence for a copper-bearing fluid in magma erupted at the Valley of Ten Thousand Smokes, Alaska. *Contrib. Mineral. Petrol.* **114**, 409–421.
- Macdonald R., Smith R. L. and Thomas J. E. (1992) Chemistry of subalkalic silicic obsidians. *U.S. Geol. Surv. Prof. Pap.*, 1523.
- Mahood G. and Hildreth W. (1983) Large partition coefficients for trace elements in high-silica rhyolites. *Geochim. Cosmochim. Acta* **47**, 11–30.
- Manley C. R. and Bacon C. R. (2000) Rhyolitic thermobarometry and the shallowing of the magma reservoir, Coso volcanic field, California. *J. Petrol.* **41**(1), 149–174.
- Markl G., von Blanckenburg F. and Wagner T. (2006) Iron isotope fractionation during hydrothermal ore deposition and alteration. *Geochim. Cosmochim. Acta* **70**, 3011–3030.
- Metz J. M. and Mahood G. A. (1991) Development of the Long Valley, California, magma chamber recorded in precaldera rhyolite lavas of Glass Mountain. *Contrib. Mineral. Petrol.* **106**, 379–397.
- Poitrasson F. (2006) On the iron isotope homogeneity of the continental crust. *Chem. Geol.* **235**, 195–200.
- Poitrasson F. and Freyrier R. (2005) Heavy iron isotope composition of granites determined by high resolution MC-ICP-MS. *Chem. Geol.* **222**, 132–147.
- Poitrasson F., Halliday A. N., Lee D. C., Levasseur S. and Teutsch N. (2004) Iron isotope differences between Earth, Moon, Mars, and Vesta as possible records of contrasted accretion mechanisms. *Earth Planet. Sci. Lett.* **223**, 253–266.
- Polyakov V. B. and Mineev S. D. (2000) The use of Mössbauer spectroscopy in stable isotope geochemistry. *Geochim. Cosmochim. Acta* **64**(5), 849–865.
- Polyakov V. B., Clayton R. N., Horita J. and Mineev S. D. (2007) Equilibrium iron isotope fractionation factors of minerals: reevaluation from the data of nuclear inelastic resonant X-ray scattering and Mössbauer spectroscopy. *Geochim. Cosmochim. Acta* **71**(15), 3833–3846.
- Rouxel O., Dobbek N., Ludden J. and Fouquet Y. (2003) Iron isotope fractionation during oceanic crust alteration. *Chem. Geol.* **202**, 155–182.
- Rouxel O., Bekker A. and Edwards K. (2005) Iron isotope constraints on the Archean and Paleoproterozoic Ocean Redox State. *Science* **307**, 1088–1091.
- Schauble E. A., Rossman G. R. and Taylor, Jr., H. P. (2001) Theoretical estimates of equilibrium Fe-isotope fractionations from vibrational spectroscopy. *Geochim. Cosmochim. Acta* **65**(15), 2487–2497.
- Schoenberg R. and von Blanckenburg F. (2006) Modes of planetary-scale Fe isotope fractionation. *Earth Planet. Sci. Lett.* **252**, 342–359.
- Schuessler J. A., Schoenberg R. and Sigmarsson O. (2007) Iron isotope fractionation during the volcanic evolution of Hekla, Iceland. *Geochim. Cosmochim. Acta* **71**(15), A907.
- Shahar A., Young E. D. and Manning C. (2008) Equilibrium high-temperature Fe isotope fractionation between fayalite and magnetite: an experimental calibration. *Earth Planet. Sci. Lett.* **268**, 330–338.
- Simon A. C., Pettke T., Candela P. A., Piccoli P. M. and Heinrich C. A. (2004) Magnetite solubility and iron transport in magmatic-hydrothermal environments. *Geochim. Cosmochim. Acta* **68**(23), 4905–4914.
- Stokey L. C. (1970) Ferrozine—a new spectrophotometric reagent for iron. *Anal. Chem.* **42**, 779–781.
- Valaas-Hyslop E., Valley J. W., Johnson C. M. and Beard B. L. (2008) The effects of metamorphism on O and Fe isotope compositions in the Biwabik iron-formation, northern Minnesota. *Contrib. Mineral. Petrol.* **155**, 313–328.
- Valley J. W., Bindeman I. N. and Peck W. H. (2003) Empirical calibration of oxygen isotope fractionation in zircon. *Geochim. Cosmochim. Acta* **67**(17), 3257–3266.
- Veksler I. V., Dorfman A. M., Kamenetsky M., Dulski P. and Dingwell D. B. (2005) Partitioning of lanthanides and Y between immiscible silicate and fluoride melts, fluorite and cryolite and the origin of the lanthanide tetrad effect in igneous rocks. *Geochim. Cosmochim. Acta* **69**(11), 2847–2860.
- Veksler I. V., Dorfman A. M., Danyushevsky L. V., Jakobsen J. K. and Dingwell D. B. (2006) Immiscible silicate liquid partition coefficients: implications for crystal-melt element partitioning and basalt petrogenesis. *Contrib. Mineral. Petrol.* **152**(6), 685–702.
- Wallace P. J., Anderson A. T. and Davis A. M. (1995) Quantification of pre-eruptive exsolved gas contents in silicic magmas. *Nature* **377**, 612–616.
- Wallace P. J., Anderson A. T. and Davis A. M. (1999) Gradients in H₂O, CO₂, and exsolved gas in a large-volume silicic magma system: interpreting the record preserved in melt inclusions from the Bishop Tuff. *J. Geophys. Res.* **104**(B9), 20097–20122.
- Webster J. D. (2004) The exsolution of magmatic hydrosaline chloride liquids. *Chem. Geol.* **210**, 33–48.
- Westrich H. R., Eichelberger J. C. and Hervig R. L. (1991) Degassing of the 1912 Katmai magmas. *Geophys. Res. Lett.* **18**(8), 1561–1564.
- Weyer S. and Ionov D. A. (2007) Partial melting and melt percolation in the mantle: the message from Fe isotopes. *Earth Planet. Sci. Lett.* **259**(1–2), 119–133.
- Weyer S., Anbar A. D., Brey G. P., Münker C., Mezger K. and Woodland A. B. (2005) Iron isotope fractionation during planetary differentiation. *Earth Planet. Sci. Lett.* **240**, 251–264.
- Whitney J. A., Hemley J. J. and Simon F. O. (1985) The concentration of iron in chloride solutions equilibrated with synthetic granitic compositions: the sulfur-free system. *Econ. Geol.* **80**, 444–460.
- Williams H., Peslier A., McCammon C., Halliday A., Levasseur S., Teutsch N. and Burg J. (2005) Systematic iron isotope variations in mantle rocks and minerals: the effect of partial melting and oxygen fugacity. *Earth Planet. Sci. Lett.* **235**, 435–452.